

Use of Small-Molecule Crystal Structures To Address Solubility in a Novel Series of G Protein Coupled Receptor 119 Agonists: Optimization of a Lead and in Vivo Evaluation

James S. Scott,^{*,†} Alan M. Birch,[†] Katy J. Brocklehurst,[†] Anders Broo,[‡] Hayley S. Brown,[†] Roger J. Butlin,[†] David S. Clarke,[†] Öjvind Davidsson,[‡] Anne Ertan,[§] Kristin Goldberg,[†] Sam D. Groombridge,[†] Julian A. Hudson,[†] David Laber,[†] Andrew G. Leach,[†] Philip A. MacFaul,[†] Darren McKerrecher,[†] Adrian Pickup,[†] Paul Schofield,[†] Per H. Svensson,[§] Pernilla Sörme,[†] and Joanne Teague[†]

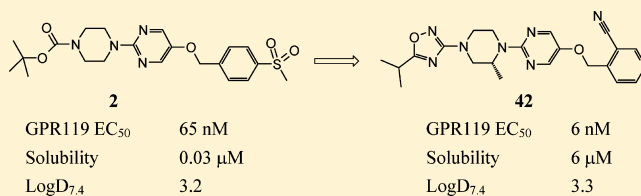
[†]Cardiovascular & Gastrointestinal Innovative Medicines Unit, AstraZeneca, Mereside, Alderley Park, Macclesfield, Cheshire SK10 4TG, United Kingdom

[‡]Cardiovascular & Gastrointestinal Innovative Medicines Unit, AstraZeneca, Pepparedsleden 1, 431 83 Mölndal, Sweden

[§]Pharmaceutical Development, AstraZeneca R&D, S-151 85 Södertälje, Sweden

S Supporting Information

ABSTRACT: G protein coupled receptor 119 (GPR119) is viewed as an attractive target for the treatment of type 2 diabetes and other elements of the metabolic syndrome. During a program toward discovering agonists of GPR119, we herein describe optimization of an initial lead compound, **2**, into a development candidate, **42**. A key challenge in this program of work was the insolubility of the lead compound. Small-molecule crystallography was utilized to understand the intermolecular interactions in the solid state and resulted in a switch from an aryl sulphone to a 3-cyanopyridyl motif. The compound was shown to be effective in wild-type but not knockout animals, confirming that the biological effects were due to GPR119 agonism.



The compound was shown to be effective in wild-type but not knockout animals, confirming that the biological effects were due to GPR119 agonism.

■ INTRODUCTION

G protein coupled receptor 119 (GPR119) is a class A type receptor that is mainly expressed in pancreatic islets and intestinal enteroendocrine cells.¹ Recent work has led to the putative identification of natural agonists of this receptor such as oleoylethanolamide (OEA)² and related compounds such as *N*-oleoyldopamine (OLDA).³ Biological studies have shown that agonism of the GPR119 receptor results in incretin secretion from the gut (e.g., glucagon-like peptide-1 (GLP-1) release from L-cells)⁴ in addition to the stimulation of insulin release from β-cells in the pancreas.⁵ This dual mechanism of action has considerable potential in the mediation of glucose homeostasis, and as a result, GPR119 agonism has been viewed with considerable interest as a novel approach to therapeutic intervention in the treatment of diabetes.^{6,7} Interest in this target was further increased by an initial disclosure by Arena that a synthetic GPR119 agonist controlled glucose excursions in preclinical animal models.⁸ A number of research groups, including Arena,⁹ GSK,¹⁰ Pfizer,¹¹ Merck,¹² and Astellas,¹³ have subsequently published their work in this area on a number of different chemotypes. Other groups are also known to be active on the basis of filed patent applications,¹⁴ and a pharmacophore model has been proposed based on similarities in structural features of published chemical series.¹⁵ A number of compounds with disclosed structures have been progressed

into clinical trials (Figure 1), including MBX-2982^{16a} (Metabolex/Sanofi-Aventis) and GSK-1292263^{16b} (GSK). The compounds APD-597 (JNJ-38431055)^{9b} and APD-668^{9b} have also been in clinical trials (Arena/Johnson & Johnson), with initial clinical data recently being published on the first of these compounds.¹⁷

We recently reported our own efforts to identify a series of GPR119 agonists that were compounded by off-target effects observed in vivo in GPR119 knockout mice.¹⁸ We herein report the synthesis and structure–activity relationships of an alternative, chemically distinct series from initial high-throughput screening hit **1** to development candidate **42**. In contrast to our previous efforts, we report that in vivo effects were observed in wild-type mice, but crucially not in GPR119 knockout mice, leading us to conclude that the biological effects observed were mediated by agonism of the GPR119 receptor.

■ RESULTS AND DISCUSSION

A high-throughput screen of the AstraZeneca compound collection identified a small cluster of hits exemplified by compound **1** (Scheme 1). This compound showed reasonable potency and intrinsic activity (IA)¹⁹ against both human (EC₅₀

Received: March 5, 2012

Published: April 30, 2012

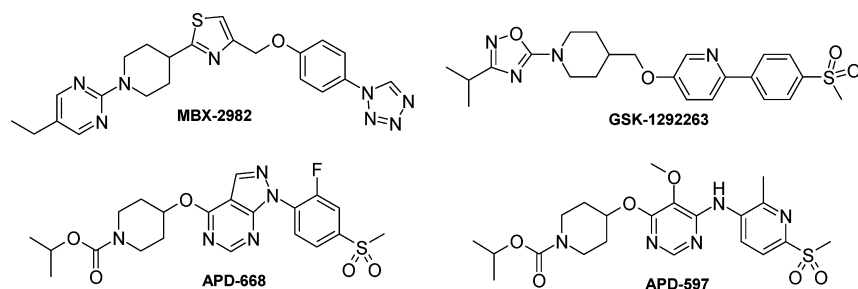


Figure 1. Structures of selected GPR119 agonists progressed into clinical development.

Scheme 1. Structures of the High-Throughput Screening Hit 1 and the Initial Lead 2

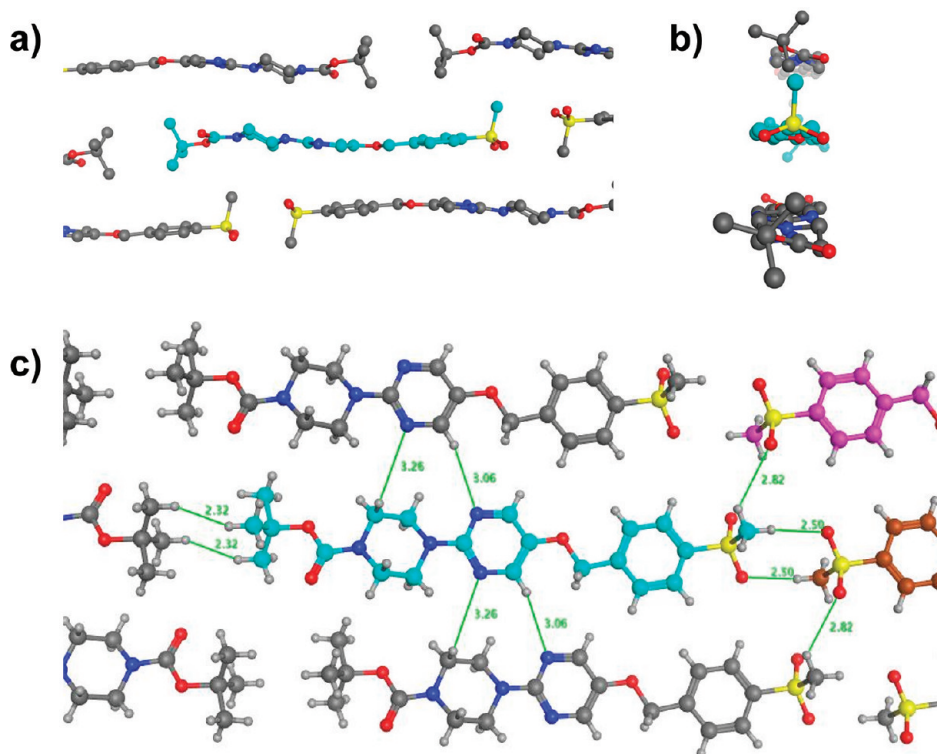
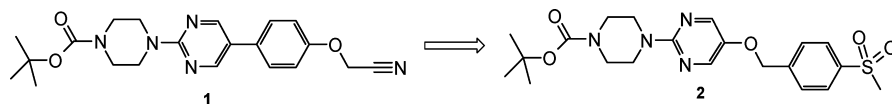
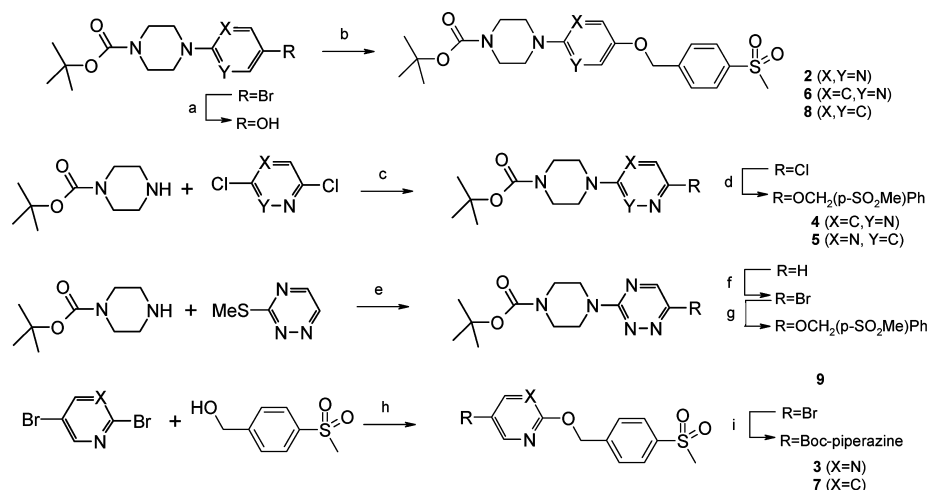


Figure 2. Three views of the X-ray structure of compound 2 showing views of the crystal packing around the molecule colored light blue. In (a) the molecule is viewed from the side, showing its flat shape and the molecules stacking above and below. In (b) the molecule is viewed from the end, showing the near vertical stacking with the molecules above and below. In (c) the molecule is shown from above, with the set of interactions shown in green that hold together the plane that stacks in (a) and (b). Distances shown are in angstroms..

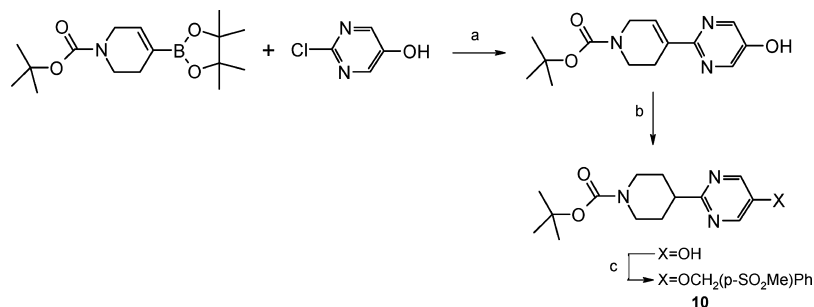
= 78 nM, IA = 81%) and murine (EC_{50} = 808 nM, IA = 78%) forms of the receptor. The lipophilicity²⁰ was high ($\log D_{7.4}$ = 4.2), leading to poor physicochemical properties²¹ (solubility <1 μ M, mouse plasma protein binding (PPB) 0.1% free) and metabolic instability in human microsomes (Cl_{int} = 259 (μ L/min)/mg). Reordering of the structure to disrupt the three contiguous rings, together with a switch from cyano to a lipophilicity-lowering sulfone resulted in the initial lead 2. This compound showed similar human potency (EC_{50} = 65 nM, IA = 83%) but much improved mouse potency (EC_{50} = 41 nM, IA = 99%) at a reduced lipophilicity ($\log D_{7.4}$ = 3.2). Improvements were also observed in the levels of free drug (mouse PPB

3.3% free) and metabolic stability in human microsomes (Cl_{int} = 47 (μ L/min)/mg), but the solubility remained low (<1 μ M).

Further experimentation revealed that compound 2 was highly insoluble (0.03 μ M) for its measured lipophilicity ($\log D_{7.4}$ = 3.2) and melting point (201–202 °C).²² To understand any interactions that contribute to the stability of the solid state²³ and hence to the low solubility, crystals of 2 suitable for X-ray structural determination were grown (Figure 2). Figure 2a shows a view from the side of one molecule of 2 (highlighted with light blue carbon) amidst the crystal lattice and illustrates how the molecule is rather flat and stacks very effectively with molecules above and below. The *tert*-butyl groups that might disrupt this packing pack together well and so do not provide

Scheme 2^a

^aReagents and conditions: (a) (i) bis(pinacolato)diborane, KOAc, Pd(OAc)₂, DMF, 85 °C, 16 h; (ii) NaBO₃·4H₂O, THF/H₂O, 25 °C, 16 h, 23–56%; (b) BrCH₂(*p*-SO₂Me)Ph, Cs₂CO₃, DMF, 40 °C, 2 h, 28–94%; (c) (iPr)₂NEt, toluene, reflux, 4 h, 26–58%; (d) HOCH₂(*p*-SO₂Me)Ph, Cs₂CO₃, CH₃CN, 150 °C, 30 h, 14–36%; (e) EtOH, 150 °C, microwave, 24 h, 63%; (f) Br₂, H₂O, 25 °C, 20 min, 74%; (g) HOCH₂(*p*-SO₂Me)Ph, Cs₂CO₃, CuI, tetramethylphenanthroline, 1,4-dioxane, 100 °C, 20 h, 9%; (h) NaH, DMF, 25 °C, 16 h, 61–87%; (i) Boc-piperazine, Pd(dba)₂, BINAP, NaO^tBu, toluene, 80 °C, 16 h, 43–55%.

Scheme 3^a

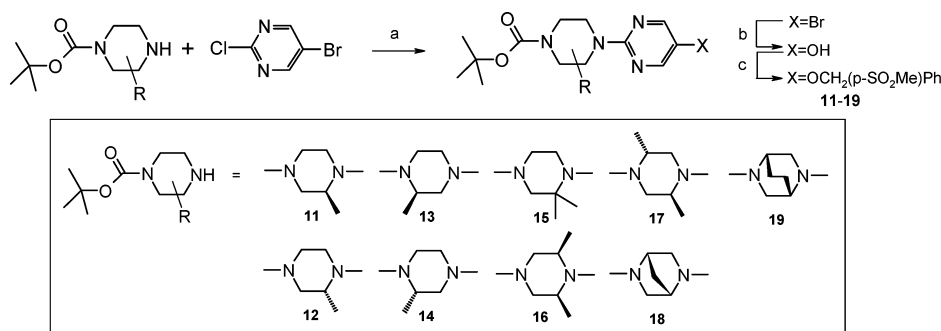
^aReagents and conditions: (a) dichloro(1,1-bis(diphenylphosphino)ferrocene)palladium(II), K₂CO₃, DME/H₂O, 85 °C, 18 h, 27%; (b) H₂, 10% Pd/C, EtOH, 20 °C, 2 h, 97%; (c) BrCH₂(*p*-SO₂Me)Ph, Cs₂CO₃, DMF, 20 °C, 18 h, 67%.

any significant disruption to the lattice. Figure 2b shows the molecule viewed from the end and illustrates how the molecules stack on top of one another. In Figure 2c an almost orthogonal view shows the molecules surrounding the light blue one along with potential interactions between them. For instance, the pyrimidine nitrogens have potential weak interactions with polarized C–H bonds in the adjacent pyrimidine ring (N–H distance ~3.06 Å) and in an adjacent piperazine ring (N–H distance ~3.26 Å). The *tert*-butyl groups stack against *tert*-butyl groups in other molecules and therefore benefit from hydrophobic interactions. Notably, the tightest set of polar interactions are between sulfone oxygens and the C–H bonds in the methyl groups in the sulfone moiety in adjacent molecules. If the *tert*-butyl groups can be said to be interacting tail-to-tail, then the sulfone groups not only interact head-to-head to form a one-dimensional chain, but also interact in an almost orthogonal direction to hold together the whole of the two-dimensional plane that then stacks as shown in Figure 2a.

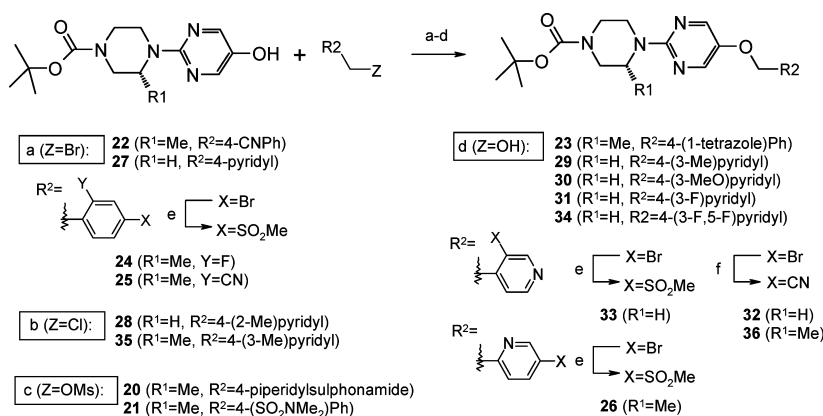
The network of interactions involving the sulfones prompted a search of the Cambridge Crystallographic Database to see if these were a common motif.²⁴ Of the methyl sulfone structures that were examined, 18% showed interactions like the head-to-head one linking the light blue molecule to the molecule to its

right shown in brown. Also, 18% showed ladderlike interactions similar to those between the light blue molecule and the molecule shown in pink. A further 23% of methyl sulfones were involved in both of these types of interaction. This left only 41% of methyl sulfones in the database that did not form either of these types of lattice interaction. A clear majority of crystal structures containing methyl sulfones involve them interacting with other methyl sulfones and the weak hydrogen bond acceptor of the sulfone interacting with at least one weak hydrogen bond donor of the C–H bonds of an adjacent methyl group.

Our medicinal chemistry strategy to improve the solubility of this lead molecule **2** was therefore to investigate the heterocyclic core and the piperazine (with a view to introducing asymmetry and disrupting edge–face interactions) followed by the aryl substituent with a view to removing the sulfone (and its associated intermolecular interactions stabilizing the solid state). Once we had identified an optimal structure, we envisaged a final round of optimization to replace the acid-labile Boc group. A compound that was potent against the mouse as well as the human receptor was viewed as essential to enable *in vivo* evaluation and to confirm that any biological effects were being mediated through GPR119 agonism. The synthetic

Scheme 4^a

^aReagents and conditions: (a) K_2CO_3 , CH_3CN , $150\text{ }^\circ\text{C}$, microwave, 1 h, 16–96%; (b) (i) bis(pinnacol)diborane, KOAc, $Pd(OAc)_2$, DMF, $85\text{ }^\circ\text{C}$, 16 h; (ii) $NaBO_3\cdot 4H_2O$, THF/ H_2O , $25\text{ }^\circ\text{C}$, 16 h, 10–78%; (c) $BrCH_2(p-SO_2Me)Ph$, Cs_2CO_3 , DMF, $40\text{ }^\circ\text{C}$, 2 h, 25–94%.

Scheme 5^a

^aReagents and conditions: (a) R^2CH_2Br , Cs_2CO_3 , CH_3CN , $100\text{ }^\circ\text{C}$, 1 h, 32–84%; (b) R^2CH_2Cl , Cs_2CO_3 , DMF, $40\text{ }^\circ\text{C}$, 2 h, 31–51%; (c) R^2CH_2OMs , Cs_2CO_3 , DMF, $55\text{ }^\circ\text{C}$, 16 h, 85–91%; (d) R^2CH_2OH , DIAD, PPh_3 , THF, $20\text{ }^\circ\text{C}$, 16 h, 27–61%; (e) CH_3SO_2Na , CuI, L-proline, NaOH, DMSO, $80\text{ }^\circ\text{C}$, 2 d, 26–58%; (f) $Zn(CN)_2$, $Pd(dba)_2$, xantphos, DMF, $130\text{ }^\circ\text{C}$, 1 h, microwave, 49–93%.

routes developed in the course of this program are described in Schemes 2–8.

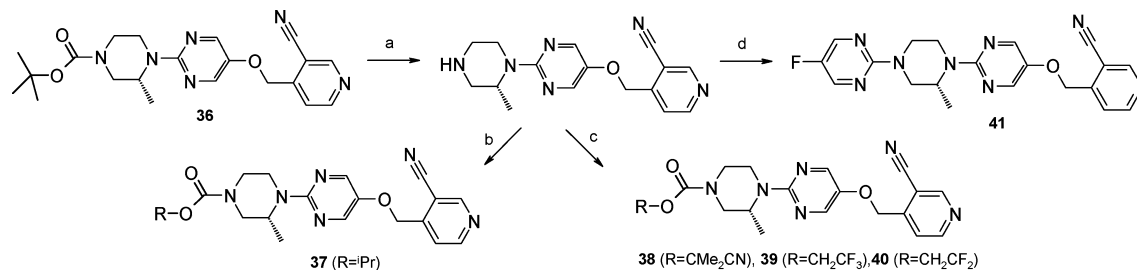
Synthesis. Synthesis of the various heterocycles (2–9) was carried out as shown in Scheme 2. Compounds 2 and 6 were synthesized from the bromides via a palladium-catalyzed borylation followed by sodium perborate oxidation to the phenol. The phenol was then alkylated using *p*-(methylsulfonyl)benzyl chloride using cesium carbonate as the base. Phenyl 8 was made via alkylation of the known phenol²⁵ (Scheme 2a). Pyridazine 4 and pyrazine 5 were made from monodisplacement of the symmetrical dichlorides with Boc-piperazine followed by displacement of the second chloride with *p*-methanesulfonylbenzyl alcohol using cesium carbonate and microwave heating (Scheme 2b). The triazine 9 was made via methanethiolate displacement with Boc-piperazine under microwave irradiation followed by a regioselective bromination and a copper-catalyzed bromide displacement with *p*-(methylsulfonyl)benzyl alcohol (Scheme 2c). Pyrimidine 3 and pyridine 7 were made from the dibromides with an initial regioselective nucleophilic aromatic substitution of the 2-bromo substituent with *p*-(methylsulfonyl)benzyl alcohol followed by a palladium-catalyzed amination with Boc-piperazine (Scheme 2d).

Piperidine 10 was made by a palladium-catalyzed coupling between the alkenyl boronate and 2-chloropyrimidin-5-ol followed by a hydrogenation of the alkene and alkylation of the phenol under standard conditions (Scheme 3).

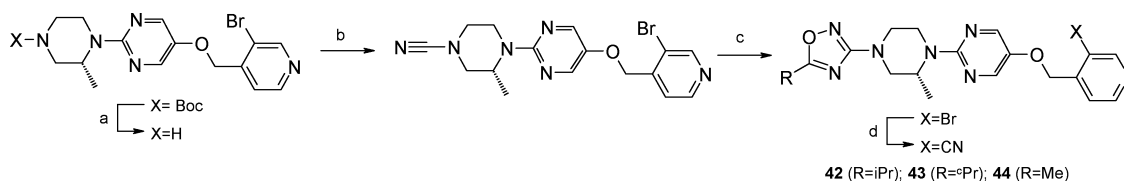
Piperidine variants 11–19 were made by nucleophilic displacement of the 2-chloro substituent of 2-chloro-5-bromopyrimidine in the presence of diisopropylethylamine as a base with microwave heating. The bromo substituent was converted to the phenol using a palladium-catalyzed borylation followed by sodium perborate oxidation. This was then alkylated using *p*-(methylsulfonyl)benzyl chloride using cesium carbonate as the base (Scheme 4).

For aryl variation, the phenols ($R^1 = H$, (*R*)-Me) were alkylated with benzylic bromides, chlorides, or mesylates to provide final compounds 22 and 27, 28 and 35, and 20 and 21, respectively (Scheme 5). For substituted sulfones 24 and 25, the intermediate aryl bromides were synthesized and then subjected to a copper-catalyzed displacement with $NaSO_2Me$. Alternatively, Mitsunobu chemistry could be used to form either final compounds (23, 29–31, 34) or a functionalized 3-bromopyridine which could be further converted to either sulfone 33 or cyanopyridyls 32 and 36. Mitsunobu chemistry was also used to build a regioisomeric bromopyridine that was treated with $NaSO_2Me$ as above to produce 26.

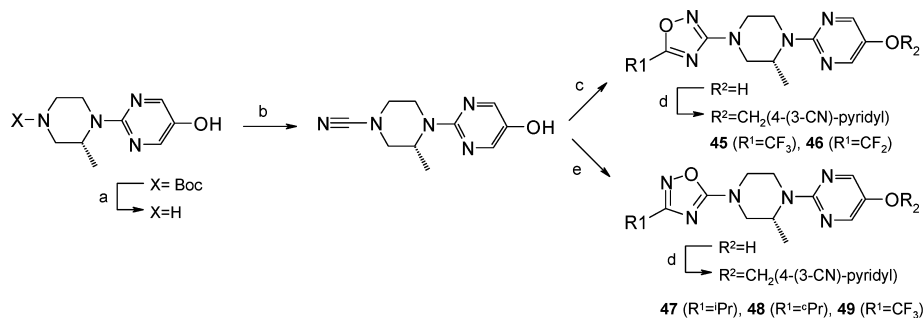
Treatment of final compound 36 with hydrochloric acid removed the Boc group and gave the piperazine salt that could be converted to carbamates by treatment with either isopropyl chloroformate (to give 37) or various phenyl carbonates to give alkyl carbamates 38–40. The amine could also be converted into heterocycles, for example, the 5-fluoropyrimidine 41, using nucleophilic aromatic substitution chemistry (Scheme 6).

Scheme 6^a

^aReagents and conditions: (a) HCl, 1,4-dioxane/CH₂Cl₂, 20 °C, 30 min, 74%; (b) ^tPrOCOCl, (^tPr)₂NEt, CH₂Cl₂, 25 °C, 16 h, 40%; (c) ROCO₂Ph, NEt₃, CHCl₃, 110 °C, 18 h, 10–39%; (d) 2-chloro-5-fluoropyrimidine, (^tPr)₂NEt, CH₃CN, 150 °C, 3 h, 29%.

Scheme 7^a

^aReagents and conditions: (a) HCl, 1,4-dioxane/CH₂Cl₂, 25 °C, 1 h 89%; (b) CNBr, NaHCO₃, CH₂Cl₂/H₂O, 25 °C, 2 h, 79%; (c) (i) NH₂OH, Na₂CO₃, DMF, 80 °C, 1 h; (ii) RCOOH, (^tPr)₂NEt, HOBt, EDAC, DMF, 20 °C, 18 h; (iii) toluene, 120 °C, 30 min, 54–66%; (d) Zn(CN)₂, Pd(dba)₂, xantphos, DMF, 130 °C, 165 min, 32–88%.

Scheme 8^a

^aReagents and conditions: (a) HCl, 1,4-dioxane/CH₂Cl₂, 20 °C, 3 d, 100%; (b) CNBr, NaHCO₃, CH₂Cl₂/H₂O, 0–25 °C, 1 h, 59%; (c) (i) NH₂OH·HCl, Na₂CO₃, DMF, 80 °C, 30 min; (ii) (R¹CO)₂O, pyridine, toluene, 45 °C, 40 min, 38–87%; (d) (4-(3-cyano)pyridyl)CH₂Cl, Cs₂CO₃, DMF, 20 °C, 70 h, 30–68%; (e) (i) R¹C(=NOH)NH₂, ZnCl₂, EtOAc/THF, 20 °C, 3 h; (ii) concentrated HCl, EtOH, 100 °C, 18 h, 47–68%.

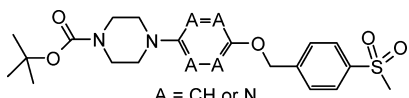
Oxadiazoles are typically synthesized via the *N*-cyanamide, but in this case, the presence of the cyanopyridyl group presented chemoselectivity issues. To circumvent this, we elected to carry the pyridyl with a bromo substituent which could be converted into the cyanide in the final step. Deprotection of the Boc group and conversion into the cyanamide using cyanogen bromide proceeded in good yield to give the key *N*-cyanamide intermediate. 3-Amino-1,2,4-oxadiazoles were constructed by treatment with hydroxylamine followed by coupling with the appropriate alkyl acid and heating to form the heterocycle. Final products 42–44 were produced through a palladium-catalyzed reaction of the pyridyl bromide with zinc cyanide (Scheme 7).

When the above sequence was attempted in the presence of (fluoroalkyl)oxadiazoles, the cyanation reactions were found to be capricious. An alternative approach was therefore devised that involved forming the heterocycle in the presence of the phenol and then alkylation to produce final compounds (Scheme 8). The Boc group was removed under acidic conditions, and then the resultant amine was reacted with

cyanogen bromide to give the cyanamide. Oxadiazole formation was carried out according to the methods described above, and then the phenol group was alkylated with the requisite chloride to produce compounds 45 and 46. This strategy was also used to produce the regioisomeric 5-amino-1,2,4-oxadiazoles 47–49 through zinc chloride mediated coupling with the requisite amidoximes followed by ring closure under acidic conditions.

Medicinal Chemistry. Our initial point of variation was the heteroaryl core of pyrimidine 2 (Table 1). The isomeric pyrimidine 3 was significantly less potent in both mouse and human assays. Of the alternative diazines, the pyridazine 4 retained some potency but lost intrinsic activity in the human assay, and in contrast, the pyrazine 5 showed no agonism at all. The pyridine isomers 6 and 7 retained submicromolar potency but were both less potent and less efficacious than the pyrimidine lead compound 2 despite being of similar lipophilicity. Removal of all heterocyclic nitrogens gave the phenyl compound 8, which, despite being the most lipophilic compound in the set, showed only weak activity at high concentrations. The triazine isomer 9 was less active than the

Table 1. Heterocyclic Core Variation



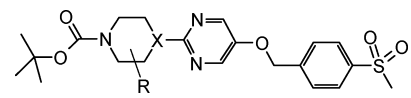
A = CH or N

Entry	Core	human GPR119 EC ₅₀ (μM)	human GPR119 IA (%)	mouse GPR119 EC ₅₀ (μM)	mouse GPR119 IA (%)	logD _{7.4}
2		0.065	83	0.041	99	3.2
3		1.084	57	1.377	20	-
4		0.485	28	1.147	69	2.8
5		>30	0	-	-	3.4
6		0.186	68	0.253	112	3.2
7		0.737	37	0.532	46	3.1
8		>7.5	62	-	-	3.9
9		0.161	61	0.226	103	2.9

original hit (EC₅₀ = 161 nM, IA = 61%) but was lower in lipophilicity (log *D*_{7.4} = 2.9), leading to a similar value for ligand-lipophilicity efficiency (LLE),^{26,27} pEC₅₀ - log *D* (3.9 vs 4.0 for **2**). On the basis of these results together with consideration of synthetic tractability, the original pyrimidine was considered optimal, and this group was fixed for further investigation.

We next turned our attention to the piperazine heterocycle of the initial lead **2** (Table 2). A switch to piperidine **10** caused a small reduction in lipophilicity (log *D*_{7.4} = 2.8)²⁸ and a large drop in potency (EC₅₀ = 893 nM), leading to an LLE reduction (3.2 vs 4.0 for **2**). A systematic variation of the methyl position on the piperazine (**11**–**14**) revealed interesting subtleties in the structure–activity relationship and also potency differences between species. Against the human receptor, the 2(*R*)-isomer **12** was the most potent (EC₅₀ = 19 nM) and showed significantly increased intrinsic activity (150%) relative to the start point **2**. Against the mouse isoform, the 2-isomers both showed similar EC₅₀ values and full agonism, but by contrast, the 3-isomers displayed only partial agonism in mouse. Substitution at the 2-position was further explored with geminal dimethyl **15**, but this resulted in a reduction in potency in human (EC₅₀ = 466 nM) and a complete loss of agonism in mouse. The 2,6-*cis*-dimethyl **16** showed a small reduction in human potency (EC₅₀ = 64 nM) but was a full agonist in mouse and was the most potent compound identified against the mouse receptor (EC₅₀ = 35 nM, IA = 95%). The 2,4-*trans*-dimethyl **17** was potent in human (EC₅₀ = 39 nM, IA = 152%) but had no murine activity. Further exploration of conformationally restricted piperazines **18** and **19** resulted in a desired reduction in lipophilicity relative to that of their methyl and dimethyl counterparts, but while **19** displayed reasonable human activity (EC₅₀ = 156 nM, IA = 85%), both showed no activity against the mouse isoform. A common theme emerging from these results was the sensitivity of the mouse receptor to alterations in this region of the molecule and in particular an intolerance for substitution proximal to the carbamate (**13**, **14**, **17**–**19**). Observations of similar effects have been reported by

Table 2. Piperazine Variation



Entry	Piperazine	human GPR119 EC ₅₀ (μM)	human GPR119 IA (%)	mouse GPR119 EC ₅₀ (μM)	mouse GPR119 IA (%)	logD _{7.4}
2		0.065	83	0.041	99	3.2
10		0.893	102	1.600	91	2.8
11		0.041	63	0.094	99	3.5
12		0.019	150	0.084	101	3.5
13		0.054	106	>30	16	>3.7
14		0.054	163	0.044	45	>3.6
15		0.466	41	>30	3	>3.6
16		0.064	104	0.035	95	>3.6
17		0.039	152	>30	3	>3.7
18		2.217	15	>30	1	2.8
19		0.156	85	>30	0	3.4

others working on GPR119 with compounds containing piperazine carbamates.^{12a} These were attributed to different conformational states, and this work further emphasizes the nuances of structural modification of ligands on GPCR pharmacology. On balance, the 2(*R*)-methyl substitution present in **12** was selected for incorporation into further compounds on the basis of the increased potency and intrinsic activity in human and mouse with comparable LLEs (4.2 vs 4.0 for **2**).

The solubility of crystalline **12** (melting point 173–174 °C) was determined experimentally and found to be 1.7 μM. Although this represents a distinct (>50-fold) improvement from the initial lead **2** (0.03 μM), the solubility remained low. To understand the effect of the methyl group on the solid state, crystals suitable for X-ray crystallography were grown. The structure of compound **12** was obtained and is shown in Figure 3. The most striking feature of this structure is that the methyl group on the piperazine adopts an axial conformation.²⁹ In Figure 3a is shown the stacking view most closely related to that in Figure 2a and in Figure 3b that most closely related to Figure 2b. These views show that while most of the molecule remains quite flat, the axial methyl group on the piperazine ring protrudes orthogonal to the plane of the molecule. The consequence of this is clear in Figure 3b, where the stacking of the molecules of **12** is significantly changed from the vertical arrangement of molecule **2** to one where the molecules are offset to accommodate the axial methyl group (which is highlighted with purple circles). In Figure 3c it is clear that although the stacking has been disrupted, the set of orthogonal

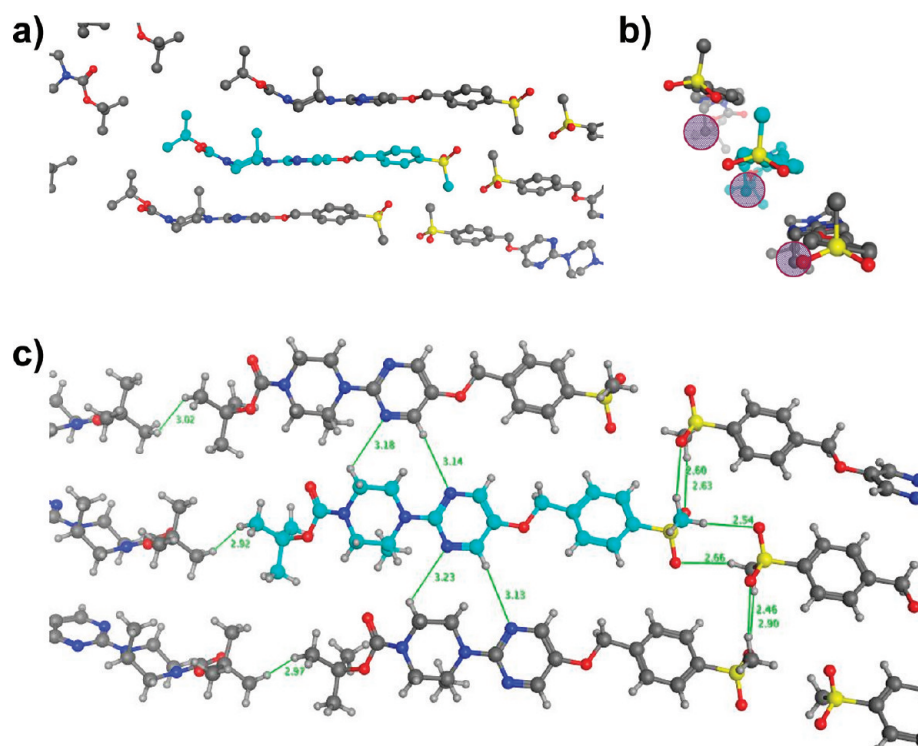


Figure 3. Three views of the X-ray structure of compound **12** showing views of the crystal packing around the molecule colored light blue. In (a) the molecule is viewed from the side along with the molecules stacking above and below. In (b) the molecule is viewed from the end, showing the significantly offset stacking with the molecules above and below; the methyl group on the piperazine is highlighted with purple circles. In (c) the molecule is shown from above, with the set of interactions shown in green that hold together the plane that stacks in (a) and (b). Distances shown are in angstroms.

interactions (hydrophobic between *tert*-butyl groups and polar between methyl sulfones) has been maintained.

An aryl sulfone is a structural motif common to a number of published GPR119 agonist chemotypes,^{9,10} and in an effort to improve the solubility of our compounds, we sought to replace it (Table 3). Piperidinesulfonamide **20** was a suitable replacement with similar potencies in both human (EC_{50} =

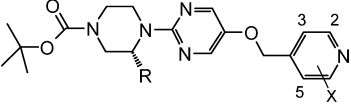
29 nM) and mouse (EC_{50} = 78 nM) and a similar LLE (4.0). By contrast, the aryl sulfonamide **21** was less potent and efficacious despite significantly increased lipophilicity. Cyano **22** and tetrazole **23** were also effective GPR119 agonists, with the tetrazole being more potent than the sulfone in both human (EC_{50} = 6 nM) and mouse (EC_{50} = 33 nM). Unfortunately, this increase in potency was achieved at the expense of increasing lipophilicity, and a $\log D_{7.4}$ > 4 was viewed as unacceptably high. A return to the sulfone and investigation of aryl variation revealed that the position *meta* to the sulfone tolerated substitution and the fluoro sulfone **24** matched the tetrazole for potency at lower $\log D_{7.4}$ (3.7), resulting in an improvement in LLE (4.8). Efforts to lower lipophilicity with a switch to cyano **25** and pyridyl **26** substitution did achieve the desired reduction in $\log D_{7.4}$ but at the expense of lower potencies and diminishing LLE (4.5 and 4.3, respectively). Notably, and in contrast to the results obtained with the piperazines, variation in this region did not lead to marked differences between potency across species. A key issue at this stage was the low aqueous solubility of the compounds (all measured as <5 μ M for **20**–**26**). This presented us with a conundrum in that although the sulfones were the most efficient groups in terms of potency/lipophilicity, they suffered from poor solubility/lipophilicity. Efforts to replace the sulfone with groups such as cyano **22** and tetrazole **23** had delivered the required potency but at the cost of higher lipophilicity, which in turn was manifest in poor solubility.

Faced with this dilemma, we elected to investigate heteroaromatic alternatives to the sulfone that contained an acceptor atom within the aryl ring, hypothesizing that this should retain the acceptor without increasing lipophilicity.

Table 3. Aryl Sulfone Variation

Entry	R	human	human	mouse	mouse	$\log D_{7.4}$	LLE (pEC_{50} - $\log D$)
		GPR119 EC_{50} (μ M)	GPR119 IA (%)	GPR119 EC_{50} (μ M)	GPR119 IA (%)		
2		0.019	150	0.084	101	3.6	4.1
20		0.029	99	0.078	67	3.5	4.0
21		0.079	66	0.264	39	>4.3	-
22		0.039	141	0.148	88	>3.6	-
23		0.006	89	0.033	115	>4.3	-
24		0.003	149	0.034	90	3.7	4.8
25		0.016	142	0.131	103	3.3	4.5
26		0.045	68	0.265	114	3	4.3

Table 4. Pyridine Variation



entry	R	X	human GPR119 EC ₅₀ (μM)	human GPR119 IA (%)	mouse GPR119 EC ₅₀ (μM)	mouse GPR119 IA (%)	log D _{7.4}	LLE (pEC ₅₀ – log D)	solubility (μM)
27	H	H	0.621	71	0.719	41	3.4	2.8	23
28	H	2-Me	>1.937	19			3.7		66
29	H	3-Me	0.075	101	0.103	60	3.8	3.3	3.8
30	H	3-OMe	1.925	22	0.071	5	3.8	1.9	11
31	H	3-F	0.063	137	1.159	157	3.6	3.6	5.1
32	H	3-CN	0.021	155	0.12	102	2.8	4.9	32
33	H	3-SO ₂ Me	>30.000	1			2.4		7
34	H	3,5-F,F	0.154	94	0.342	70	3.7	3.1	11
35	Me	3-Me	0.184	68	0.236	60	3.8	2.9	45
36	Me	3-CN	0.005	171	0.036	97	3.3	5.0	24

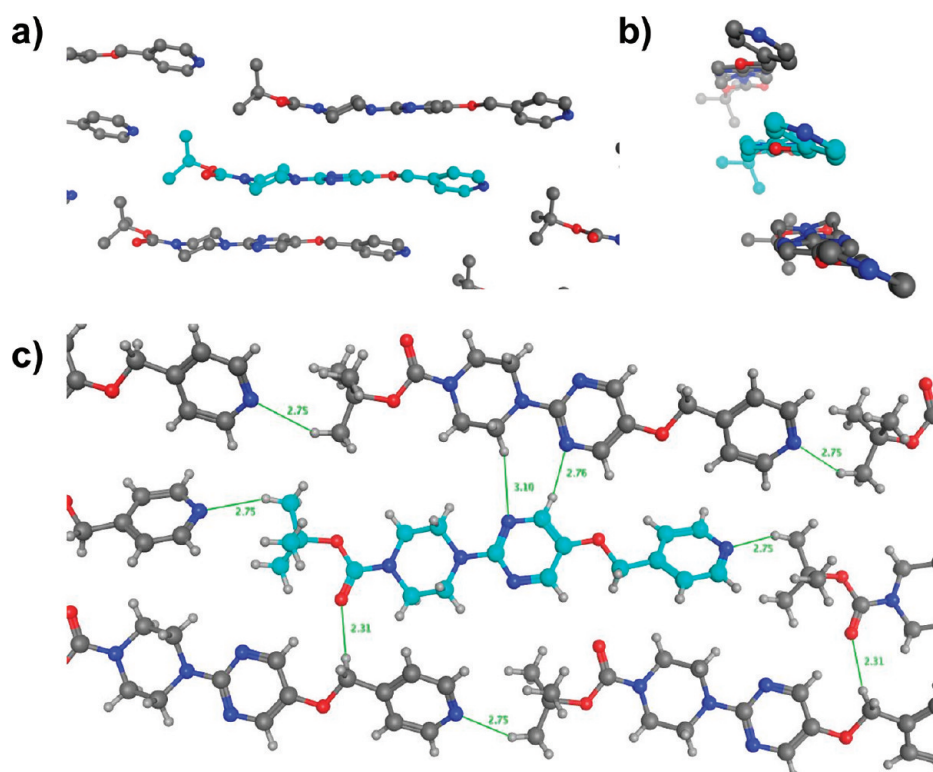


Figure 4. Three views of the X-ray structure of compound 27 showing views of the crystal packing around the molecule colored light blue. In (a) the molecule is viewed from the side along with the molecules stacking above and below. In (b) the molecule is viewed from the end, showing the slightly offset stacking with the molecules above and below. In (c) the molecule is shown from above, with the set of interactions shown in green that hold together the plane that stacks in (a) and (b). Distances shown are in angstroms.

Initial work was carried out in the unsubstituted piperazine series, and the pyridine 27 in which the hydrogen bond acceptor present in the sulfone of 2 is replaced with a pyridyl nitrogen was quickly identified. This was notable for having significantly improved solubility (23 μM) at a similar log D_{7.4} (3.4) but lower melting point (147–148 °C) compared to the sulfone 12 (Table 4). Crystallography was again used to understand the solid-state interactions, and the structure that was obtained is shown in Figure 4.

Figure 4a shows that 27 adopts a flat shape like that of 2 shown in Figure 2a. Figure 4b shows that the stacking of 27, while not directly on top of one another as for 2 in Figure 2b, is not offset to the same degree as that of the methylated 12 in

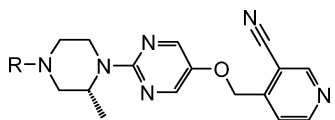
Figure 3b. The most striking difference between the structure of compound 27 and those of the two sulfones in Figures 2 and 3 is the absence of the network of weak polar interactions that the methyl sulfone is able to form. This presumably contributes to the lower melting point and to the solubility improvements for pyridyl compounds compared to the corresponding methyl sulfones of similar lipophilicities.

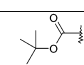
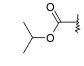
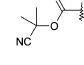
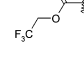
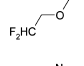
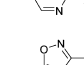
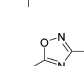
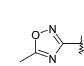
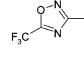
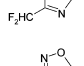
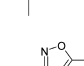
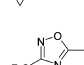
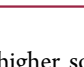
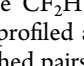
Unfortunately, the human potency of 27 was significantly compromised (EC₅₀ = 621 nM, IA = 71%), leading to an erosion in the LLE (2.8). Substitution with a methyl group at the 2-position (28) resulted in a loss of activity. However, at the 3-position (29), methyl significantly improved potency (EC₅₀ = 75 nM, IA = 101%), leading to an increase in LLE

(3.3). An exploration of groups at the 3-position (30–33) identified that the cyano group **32** had the doubly desirable effect of significantly increasing potency ($EC_{50} = 21$ nM, IA = 155%) while simultaneously lowering $\log D_{7.4}$ (2.8). This led to an increase in LLE (4.9) and maintained the good solubility (32 μ M). Substitution on both sides of the aromatic ring exemplified by the 3,5-difluoropyridyl **34** did not significantly increase either potency or solubility. Similar pyridyl substitution in the 2(R)-methylpiperazine series (**35** and **36**) showed additivity in the SAR, leading to compound **36** that had potency and intrinsic activity ($EC_{50} = 5$ nM, IA = 171%) comparable to those of either the tetrazole **23** or fluorosulfone **24** but with markedly improved solubility (24 μ M vs <5 μ M). It is notable that although the structural difference between pyridines **27** and **36** is merely the addition of a methyl and a cyano group, and while the compounds have similar measured solubility and $\log D_{7.4}$ values, pyridine **36** is over 100 times more potent than the starting point **27** as reflected in the high LLE (5.0).

Our final task in the optimization of this series involved replacement of the Boc group, and our initial focus was on the alkyl substituent of the carbamate (Table 5). The isopropyl carbamate **37** was significantly less potent but showed greater stability under acidic conditions than the *tert*-butyl carbamate **36**. The cyano analogue **38** showed a significant reduction in potency (EC_{50} 50 nM) but a concomitant drop in $\log D_{7.4}$ (2.3) in line with a constant LLE (5.0). Disappointingly, the reduction in lipophilicity did not result in increased solubility (9 μ M). The trifluoroethyl carbamate **39** showed only a small decrease in potency ($EC_{50} = 20$ nM, IA = 132%) with solubility (23 μ M) and LLE (4.7) similar to those of **36**. Fluorination at the β -position relative to an oxygen atom can have profound effects on the lipophilicity,³⁰ and in this case difluoroethyl carbamate **40** resulted in a significant reduction in $\log D_{7.4}$ ($\Delta \log D_{(CF_3-CHF_2)} = 0.7$) and a corresponding drop in potency ($EC_{50} = 100$ nM) in line with a constant LLE (4.7). In common with **38**, however, no benefits were observed in terms of improved solubility. Certain heterocycles are well-known isosteres of carbamates, and this tactic has been used by other groups in their efforts to develop agonists of GPR119.^{9,10} We found that six-membered heterocycles as exemplified by pyrimidine **41** suffered a dramatic fall in solubility (<1 μ M) that we attributed to the symmetry and rigidity of the three contiguous rings. A move to the less symmetrical five-membered heterocycles, such as isopropylloxadiazole **42** resulted in a compound that was approximately equipotent ($EC_{50} = 8$ nM, IA = 269%) and isolipophilic (3.3) with the Boc carbamate **36** with only a small erosion in terms of solubility (6 μ M). Close analogues such as the cyclopropyl **43** retained potency; however, trimming of the alkyl substituent to methyl **44** resulted in a worsening of LLE (4.0), although the reduced lipophilicity did increase the measured solubility (64 μ M). The (trifluoromethyl)oxadiazole **45** resulted in the most potent and efficacious human GPR119 agonist identified in this series ($EC_{50} = 2$ nM, IA = 243%) but at the expense of a higher than desired $\log D_{7.4}$ (4.0). Efforts to lower lipophilicity by switching to the (difluoromethyl)oxadiazole **46** resulted in a dramatic reduction of $\log D_{7.4}$ ($\Delta_{(CF_3-CHF_2)} = 1.1$) and constant LLE (4.7), however no apparent benefit in terms of solubility (5 μ M). The contrast between the (difluoromethyl)oxadiazole **46** and methylloxadiazole **44** is noteworthy in that they are of similar lipophilicity and yet the methyl compound exhibits >10-

Table 5. Carbamate and Heterocycle Variation



Entry	R	human	human	mouse	mouse	$\log D_{7.4}$	LLE	Solubility
		GPR119	GPR119	GPR119	GPR119			
		EC_{50}	IA	EC_{50}	IA	(pEC ₅₀ -		(μ M)
		(μ M)	(%)	(μ M)	(%)	logD)		
36		0.005	171	0.036	97	3.3	5.0	24
37		0.112	171	0.458	77	-	-	-
38		0.054	125	1.055	122	2.3	5.0	9
39		0.020	132	0.246	76	3.0	4.7	23
40		0.100	196	0.634	43	2.3	4.7	14
41		0.063	104	0.567	63	3.4	3.8	<0.6
42		0.008	269	0.056	92	3.3	4.8	6
43		0.014	161	0.089	45	3.1	4.8	4.8
44		0.234	192	>8.164	64	2.6	4.0	64
45		0.002	243	0.051	102	4.0	4.7	3
46		0.021	240	0.211	47	2.9	4.8	3
47		0.010	199	0.091	70	3.1	4.9	13
48		0.025	224	0.158	49	3.5	4.2	14
49		0.005	236	0.091	61	3.1	5.2	5

fold higher solubility potentially due to solid-state interactions of the CF_2H group.³¹ The isomeric oxadiazoles **47–49** were also profiled and found to be marginally less potent than their matched pairs with the same rank order of substituents in terms of potency ($CF_3 > {}^iPr > {}^nPr$). The (trifluoromethyl)oxadiazole **49** represents the most efficient compound in terms of LLE (5.2) and shows a remarkable reduction in $\log D_{7.4}$ (–0.9) relative to its positional isomer **45** that has been attributed to differences in hydrogen bond acceptor strength.³¹

Compound **42** was selected for further profiling and evaluation in terms of its suitability for further development. The compound displayed no inhibition toward five major isoforms of cytochrome P450 enzymes (CYP1A2, CYP2C9, CYP2C19, CYP2D6, and CYP3A4) in a high-throughput fluorescence assay, with IC_{50} values >30 μ M. Plasma protein

binding was consistent across species (mouse, 1.9% free; rat, 1.8% free; dog, 2.0% free; human, 1.3% free). Compound **42** exhibited low solubility as measured on crystalline material (6 μM) but good cellular permeability as measured in an *in vitro* CACO-2 assay (apical to basolateral $P_{\text{app}} = 85 \times 10^{-6}$ cm/s at a compound concentration of 10 μM) with no evidence of efflux. In contrast to Boc-containing compounds such as **12**, compound **42** showed no evidence of hydrolytic instability across the pH range 1–10. Weak activity was observed against the hERG channel ($\text{IC}_{50} = 10 \mu\text{M}$);³² however, the high margin (>1000) relative to primary potency and lack of activity against other ion channels screened (NaV_{1.5}, IKs, Ito, CaV_{1.2}) gave us confidence to progress this compound further. Compound **42** was relatively clean against a panel of 167 other targets, with only four hits (acetylcholinesterase, adenosine transporter, SHT2B, and vesicular monoamine transporter 2) showing between 50% and 75% activity at 10 μM .

Pharmacokinetic parameters (intravenous (iv) and per os (po)) for compound **42** were determined in C57BL6 mice, Han Wistar rats, and beagle dogs. The compound was administered orally as a suspension in aqueous 0.1% (w/v) pluronic F127 at relevant pharmacological doses (2–13 mg/kg). As shown in Table 6, compound **42** displayed modest

Table 6. Pharmacokinetic Parameters for Compound 42^a

species	Cl_p [(mL/min)/kg]	V_{ss} (L/kg)	po half- life (h)	iv half- life (h)	F_{abs}	bioavailability (%)
mouse	49	2.4	1	1	0.3	22
rat	28	5.1	6	3	0.5	29
dog	3.6	4.1	5	11	0.3	24

^aCompounds were dosed at 2 mg/kg (iv) and 5 mg/kg (po, mouse and rat) and 13 mg/kg (po, dog) in 5% DMSO/95% (hydroxypropyl)- β -cyclodextrin and a 0.1% pluronic F127 suspension, respectively, at volumes of 5 mL/kg (mouse and rat) and 2 mL/kg (dog).

fraction absorbed (F_{abs}) and bioavailability (F) across the three preclinical species. The volume of distribution (V_{ss}) was relatively constant across the three species. Clearance (Cl_p) was high in the rodent species and low in dog. This was consistent with *in vitro* measurements that showed that compound **42** is metabolically unstable in mouse and rat hepatocytes ($\text{Cl}_{\text{int}} = 67$ and 29 ($\mu\text{L}/\text{min})/10^6$ cells, respectively) yet relatively stable in dog hepatocytes ($\text{Cl}_{\text{int}} = 5.6$ ($\mu\text{L}/\text{min})/10^6$ cells). In bile duct cannulated rats, compound **42** was found to be eliminated predominantly by metabolism, with no parent compound detected in bile or urine. This was consistent with the good *in vitro*–*in vivo* correlations of metabolic clearance observed in all three preclinical species.

Table 7. Exposure from Rising Dose Pharmacokinetic Studies for Compound 42^a

species	dose (mg/kg)	C_{max} (μM)	AUC_{0-t} ($\mu\text{M}\cdot\text{h}$)	species	dose (mg/kg)	C_{max} (μM)	AUC_{0-t} ($\mu\text{M}\cdot\text{h}$)
mouse	5	0.4	0.7	dog	1	0.6	4.0
mouse	30	3.5	6.4	dog	5	2.5	14
mouse	100	14	42	dog	10	1.3	11
rat	5	0.7	2.7	dog	50	10	119
rat	100	6.3	97				

^a AUC_{0-t} is AUC_{0-24} in all rat and dog studies; however, due to LOQ issues in the mouse as a result of the microsampling technique, the 30 mg/kg dose is AUC_{0-6} and the 5 and 100 mg/kg doses are AUC_{0-12} .

The low bioavailability and solubility of this compound caused concern that dose escalation would not lead to an increase in exposure, potentially precluding further *in vivo* evaluation in preclinical toxicity studies. As a consequence, high-dose pharmacokinetic studies were carried out in all three preclinical species on fully crystalline material (as judged by X-ray powder diffraction). Pleasingly, the results shown in Table 7 show significant increases in exposure up to 100 mg/kg in rodents and up to 50 mg/kg in dog (Table 7).

Compound **42** was investigated *in vivo* for its potential to control the glucose excursion in a mouse (C57BL6/JAX) oral glucose tolerance test (OGTT).³³ As shown in Figure 5a, **42** significantly enhances glucose disposal at doses of 5 mg/kg and above. In separate experiments, the amount of total GLP-1 in systemic circulation was measured as a more proximal pharmacodynamic marker of GPR119 receptor agonism. In lean mice, **42** increases total GLP-1 levels 30 min after oral administration of the compound, with statistically significant increases observed at doses of 10 mg/kg and above (Figure 5b).

To verify that the pharmacodynamic effects were indeed mediated through GPR119 agonism, compound **42** was tested in both wild-type (WT) and GPR119 knockout (KO) mice. In stark contrast to results obtained with a previous series,¹⁸ **42** showed no effect on either glucose disposal (at a dose of 100 mg/kg) or GLP-1 secretion (at a dose of 50 mg/kg) in the knockout mice, with wild-type controls displaying the expected response (Figure 6).

Having demonstrated that compound **42** enhances glucose disposal and GLP-1 secretion at a dose of 15 mg/kg, we studied the pharmacology of compound **42** in conjunction with the dipeptidyl peptidase-4 (DPP-IV) inhibitor sitagliptin at a dose of 1 mg/kg. DPP-IV inhibitors prevent inactivation of GLP-1 to an inactive form,³⁴ and our hypothesis was that this would augment the effects of our GPR119 agonist. As shown in Figure 7, in the mouse OGTT the glucose lowering achieved with the combination demonstrates a clear, statistically significant benefit of the combination over each monotherapy. On the basis of the overall compound profile and the encouraging *in vivo* results, **42** was selected as a candidate for further development, the results of which will be reported in due course.

CONCLUSION

In conclusion, we have described the optimization of an initial lead compound, **2**, into a development candidate, **42**. A key challenge in this program of work was the insolubility of the lead compound. Small-molecule crystallography was utilized to understand the intermolecular interactions in the solid state and resulted in a switch from an aryl sulfone to a 3-cyanopyridyl motif. Compound **42** was shown to be effective

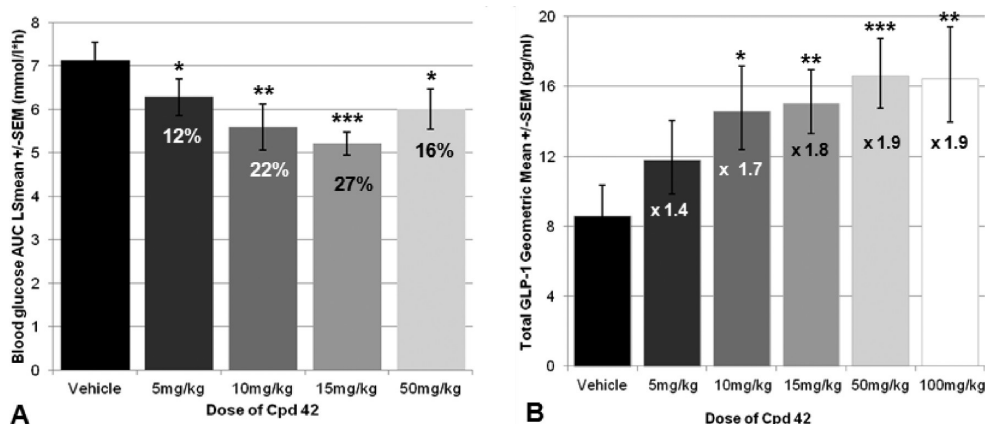


Figure 5. Oral administration of compound 42 enhances glucose disposal and GLP-1 secretion in lean mice. (A) Percent reduction in OGTT blood glucose AUC. Compound 42 was administered 30 min prior to a glucose load of 2 g/kg, and glucose levels were monitored for 90 min. (B) Fold increase in GLP-1 secretion. Compound 42 was administered to fasted animals 30 min prior to terminal blood sampling for total GLP-1 levels.

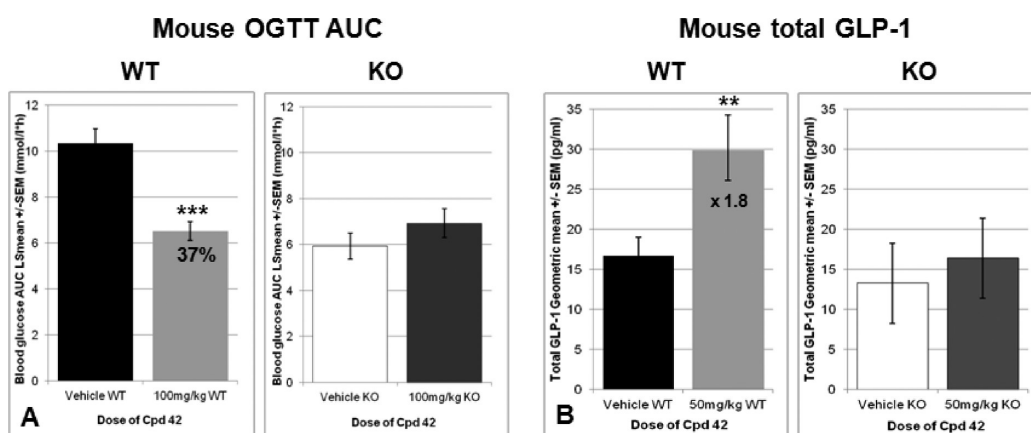


Figure 6. Compound 42 enhances glucose disposal (OGTT) and GLP-1 secretion in WT but not GPR119 KO mice. (A) Percent reduction in OGTT blood glucose AUC. Compound 42 was administered 30 min prior to a glucose load of 2 g/kg, and glucose levels were monitored for 90 min. (B) Fold increase in GLP-1 secretion. Compound 42 was administered to fasted animals 30 min prior to terminal blood sampling for total GLP-1 levels.

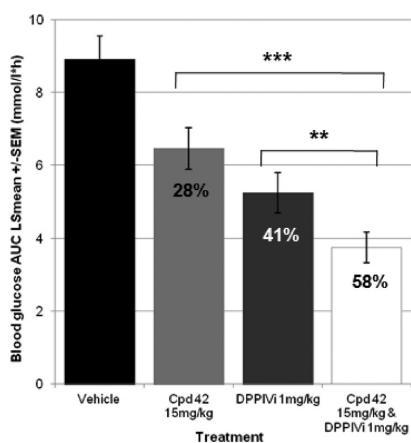


Figure 7. Combination of compound 42 and sitagliptin shows benefit in glucose disposal over monotherapy. Percent reduction in OGTT blood glucose AUC. Compound 42 (15 mg/kg) and/or sitagliptin (1 mg/kg) was administered 30 min prior to a glucose load of 2 g/kg, and glucose levels were monitored for 90 min.

in WT but not KO animals, confirming that the biological effects were due to GPR119 agonism.

EXPERIMENTAL SECTION

General Procedures. All solvents and chemicals used were reagent grade. Flash column chromatography was carried out using prepacked silica cartridges (from 4 to 330 g) from Rediseq, Biotage, or Crawford and eluted using an Isco Companion system. ^1H NMR were recorded on a Bruker Avance DPX400 (400 MHz) and were determined in CDCl_3 or $\text{DMSO}-d_6$. ^{13}C NMR spectra were recorded at 101 or 175 MHz. Chemical shifts are reported in parts per million relative to the peak for tetramethylsilane (TMS) (0.00 ppm) or solvent peaks as the internal reference, and coupling constant (J) values are reported in hertz. Splitting patterns are indicated as follows: s, singlet; d, doublet; t, triplet; m, multiplet. Merck precoated thin-layer chromatography (TLC) plates (silica gel 60 F_{254} , 0.25 mm, article 5715) were used for TLC analysis. The purity of compounds submitted for screening was >95% as determined by UV analysis of liquid chromatography–mass spectroscopy (LC–MS) chromatograms at 254 nm and substantiated using the TAC (total absorption chromatogram). Further support for the purity statement was provided using the MS TIC (total ion current) trace in ESI +ve and –ve ion modes, HRMS, and NMR analysis. Solutions were dried over anhydrous magnesium sulfate, and solvent was removed by rotary evaporation under reduced pressure. Optical rotations were measured on a polarimeter at a wavelength of 589 nm corresponding to the sodium D-line in solutions of methanol. Melting points were determined on a Mettler FP62 automatic melting point apparatus. Representative compounds (12, 42, 45) were examined by X-ray

powder diffraction and found to have sharp peaks indicative of crystalline compounds.

tert-Butyl 4-(5-[[4-(Methylsulfonyl)benzyl]oxy]pyrimidin-2-yl)piperazine-1-carboxylate (2). Cesium carbonate (2.092 g, 6.42 mmol) was added to *tert*-butyl 4-(5-hydroxypyrimidin-2-yl)piperazine-1-carboxylate (0.6 g, 2.14 mmol) and 1-(bromomethyl)-4-(methylsulfonyl)benzene (0.587 g, 2.35 mmol) in DMF (10 mL). The resulting mixture was stirred at 40 °C for 2 h. The reaction mixture was quenched with water (150 mL) and extracted with Et₂O (2 × 200 mL), and the organic layer was dried over MgSO₄, filtered, and evaporated to afford a cream solid. Upon addition of water and EtOAc/ether, a white solid was filtered off and dried. The cream solid was triturated with CH₂Cl₂ to give a white solid. The two white solids were combined to give *tert*-butyl 4-(5-[[4-(methylsulfonyl)benzyl]oxy]pyrimidin-2-yl)piperazine-1-carboxylate (0.421 g, 43%): mp 201–202 °C; ¹H NMR (400 MHz, DMSO) δ 8.30 (s, 2H), 7.96 (d, *J* = 8.4 Hz, 2H), 7.71 (d, *J* = 8.3 Hz, 2H), 5.25 (s, 2H), 3.62 (dd, *J* = 6.2, 4.2 Hz, 4H), 3.42–3.35 (m, 4H), 3.22 (s, 3H), 1.43 (s, 9H); HRMS (ESI) calcd for C₂₁H₂₉O₅N₄S (M + H)⁺ 449.1853, found 449.1852.

tert-Butyl 4-(2-[[4-(Methylsulfonyl)benzyl]oxy]pyrimidin-5-yl)piperazine-1-carboxylate (3). 5-Bromo-2-(4-(methylsulfonyl)benzyloxy)pyrimidine (748.8 mg, 2.18 mmol), *tert*-butyl piperazine-1-carboxylate (447 mg, 2.40 mmol), tris(dibenzylideneacetone)dipalladium(0) (100 mg, 0.11 mmol), 2,2'-bis(diphenylphosphino)-1,1'-binaphthyl (67.9 mg, 0.11 mmol), and sodium 2-methylpropano-2-olate (315 mg, 3.27 mmol) were mixed with toluene (20 mL). Nitrogen was bubbled through the solvent for 15 min, and the resulting mixture was stirred at 80 °C for 16 h. The reaction mixture was filtered through Celite, then evaporated to dryness, redissolved in EtOAc (75 mL), and washed sequentially with water (2 × 75 mL) and saturated brine (100 mL). The organic layer was dried over MgSO₄, filtered, and evaporated to afford crude product that was purified by flash silica chromatography, elution gradient 0–100% EtOAc in isohexane and then by preparative HPLC (Phenomenex Gemini C18 110A (axia) column, 5 μm silica, 21 mm diameter, 150 mm length) using decreasingly polar mixtures of water (containing 0.5% NH₃ and MeCN) as eluents. Fractions containing the desired compound were evaporated to dryness to afford *tert*-butyl 4-(2-[[4-(methylsulfonyl)benzyl]oxy]pyrimidin-5-yl)piperazine-1-carboxylate (0.538 g, 55%) as a white solid: ¹H NMR (400 MHz, CDCl₃) δ 8.20 (s, 2H), 7.93 (d, *J* = 8.4 Hz, 2H), 7.67 (d, *J* = 8.2 Hz, 2H), 5.48 (s, 2H), 3.65–3.50 (m, 4H), 3.05 (m, 7H), 1.48 (s, 9H); HRMS (ESI) calcd for C₂₁H₂₉O₅N₄S (M + H)⁺ 449.1853, found 449.1850.

tert-Butyl 4-(6-[[4-(Methylsulfonyl)benzyl]oxy]pyridazin-3-yl)piperazine-1-carboxylate (4). To a stirred solution of *tert*-butyl 4-(6-chloropyridazin-3-yl)piperazine-1-carboxylate (300 mg, 1.00 mmol) and 4-(methylsulfonyl)benzyl alcohol (224 mg, 1.20 mmol) in acetonitrile (10 mL) in a microwave vial was added cesium carbonate (981 mg, 3.01 mmol). The stirred mixture was heated at 150° for a total of 30 h and then cooled to ambient temperature. The solvent was evaporated to give a residue which was partitioned between ethyl acetate (100 mL) and water (50 mL), and the ethyl acetate layer was washed with brine, dried (MgSO₄), and evaporated to give a residue which was chromatographed on silica with 75% ethyl acetate in isohexane as the eluant and then crystallized from methanol to give *tert*-butyl 4-(6-[[4-(methylsulfonyl)benzyl]oxy]pyridazin-3-yl)piperazine-1-carboxylate (63.0 mg, 14%): mp 208–209 °C; ¹H NMR (400 MHz, CDCl₃) δ 7.87 (d, *J* = 8.4 Hz, 2H), 7.59 (d, *J* = 8.4 Hz, 2H), 6.99 (d, *J* = 9.6 Hz, 1H), 6.89 (d, *J* = 9.6 Hz, 1H), 5.50 (s, 2H), 3.56–3.36 (m, 8H), 2.97 (s, 3H), 1.42 (s, 9H); HRMS (ESI) calcd for C₂₁H₂₉O₅N₄S (M + H)⁺ 449.1853, found 449.1849.

tert-Butyl 4-(5-[[4-(Methylsulfonyl)benzyl]oxy]pyrazin-2-yl)piperazine-1-carboxylate (5). Compound 5 was synthesized as described for 2 using *tert*-butyl 4-(5-chloropyrazin-2-yl)piperazine-1-carboxylate as the starting material in 36% yield: ¹H NMR (400 MHz, CDCl₃) δ 7.98–7.91 (m, 2H), 7.69 (s, 1H), 7.65 (s, 1H), 7.64–7.59 (m, 2H), 5.41 (s, 2H), 3.52 (s, 8H), 3.05 (s, 3H), 1.49 (s, 9H); HRMS (ESI) calcd for C₂₁H₂₉O₅N₄S (M + H)⁺ 449.1853, found 449.1850.

tert-Butyl 4-(5-[[4-(Methylsulfonyl)benzyl]oxy]pyridin-2-yl)piperazine-1-carboxylate (6). Compound 6 was synthesized as

described for 2 using *tert*-butyl 4-(5-hydroxypyridin-2-yl)piperazine-1-carboxylate as the starting material in 28% yield: ¹H NMR (400 MHz, CDCl₃) δ 8.00–7.93 (m, 3H), 7.62 (d, *J* = 8.5 Hz, 2H), 7.20 (dd, *J* = 3.1, 9.1 Hz, 1H), 6.64 (d, *J* = 9.1 Hz, 1H), 5.13 (s, 2H), 3.59–3.59 (m, 4H), 3.45–3.36 (m, 4H), 3.05 (s, 3H), 1.48 (s, 9H); HRMS (ESI) calcd for C₂₂H₃₀O₅N₃S (M + H)⁺ 448.1901, found 448.1898.

tert-Butyl 4-(6-[[4-(Methylsulfonyl)benzyl]oxy]pyridin-3-yl)piperazine-1-carboxylate (7). Compound 7 was synthesized as described for 3 using 5-bromo-2-(4-(methylsulfonyl)benzyloxy)pyridine as the starting material in 43% yield: ¹H NMR (400 MHz, CDCl₃) δ 7.96–7.89 (m, 2H), 7.76 (d, *J* = 2.8 Hz, 1H), 7.63 (d, *J* = 8.5 Hz, 2H), 7.32 (dd, *J* = 9.0, 3.0 Hz, 1H), 6.82–6.75 (m, 1H), 5.43 (s, 2H), 3.71–3.50 (m, 4H), 3.03 (d, *J* = 8.4 Hz, 7H), 1.48 (s, 9H); HRMS (ESI) calcd for C₂₂H₃₀O₅N₃S (M + H)⁺ 448.1900, found 448.1897.

tert-Butyl 4-(4-[[4-(Methylsulfonyl)benzyl]oxy]phenyl)piperazine-1-carboxylate (8). Compound 8 was synthesized as described for 2 using *tert*-butyl 4-(4-hydroxyphenyl)piperazine-1-carboxylate as the starting material in 94% yield: mp 190–191 °C; ¹H NMR (400 MHz, CDCl₃) δ 7.88 (d, *J* = 8.4 Hz, 2H), 7.56 (d, *J* = 8.5 Hz, 2H), 6.82 (s, 4H), 5.04 (s, 2H), 3.56–3.46 (m, 4H), 2.98 (s, 3H), 2.97–2.92 (m, 4H), 1.41 (s, 9H); HRMS (ESI) calcd for C₁₃H₃₁O₅N₂S (M + H)⁺ 447.1948, found 447.1944.

tert-Butyl 4-(6-[[4-(Methylsulfonyl)benzyl]oxy]-1,2,4-triazin-3-yl)piperazine-1-carboxylate (9). To a stirred suspension of 4-(methylsulfonyl)benzyl alcohol (465 mg, 2.50 mmol), *tert*-butyl 4-(6-bromo-1,2,4-triazin-3-yl)piperazine-1-carboxylate (172 mg, 0.50 mmol), 3,4,7,8-tetramethyl-1,10-phenanthroline (23.62 mg, 0.10 mmol), copper(I) iodide (9.52 mg, 0.05 mmol), and cesium carbonate (488 mg, 1.50 mmol) in a microwave vial was added 1,4-dioxane (5 mL). The mixture was heated at 100 °C for 20 h and cooled to ambient temperature, and the dioxane was evaporated in vacuo to a residue which was treated with saturated ammonium chloride solution (15 mL) and extracted with ethyl acetate (3 × 15 mL). The combined ethyl acetate extracts were washed with brine, dried (MgSO₄), and evaporated in vacuo to a residue which was chromatographed on silica with 50% ethyl acetate in isohexane as the eluant and then by reversed-phase chromatography to give *tert*-butyl 4-(6-[[4-(methylsulfonyl)benzyl]oxy]-1,2,4-triazin-3-yl)piperazine-1-carboxylate (21 mg, 9%): ¹H NMR (400 MHz, CDCl₃) δ 8.02 (s, 1H), 7.89 (d, *J* = 8.4 Hz, 2H), 7.59 (d, *J* = 8.5 Hz, 2H), 5.47 (s, 2H), 3.73–3.42 (m, 8H), 2.98 (s, 3H), 1.42 (s, 9H); HRMS (ESI) calcd for C₂₀H₂₈O₅N₅S (M + H)⁺ 450.1806, found 450.1803.

tert-Butyl 4-(5-[[4-(Methylsulfonyl)benzyl]oxy]pyrimidin-2-yl)piperidine-1-carboxylate (10). Cesium carbonate (303 mg, 0.93 mmol) was added to *tert*-butyl 4-(5-hydroxypyrimidin-2-yl)piperidine-1-carboxylate (130 mg, 0.47 mmol) and 4-(methylsulfonyl)benzyl chloride (105 mg, 0.51 mmol) in DMF (7.0 mL). The resulting suspension was stirred at 20 °C for 18 h. It was diluted with ethyl acetate (100 mL), washed with water (20 mL) and brine (20 mL), dried (MgSO₄), concentrated in vacuo, and adsorbed onto silica. The crude product was purified by flash silica chromatography, elution gradient 0–100% EtOAc in isohexane. Pure fractions were evaporated to dryness to afford *tert*-butyl 4-(5-[[4-(methylsulfonyl)benzyl]oxy]pyrimidin-2-yl)piperidine-1-carboxylate (140 mg, 67%) as a white solid: mp 144–145 °C; ¹H NMR (400 MHz, DMSO) δ 8.56 (s, 2H), 7.96 (d, *J* = 8.3 Hz, 2H), 7.73 (d, *J* = 8.2 Hz, 2H), 5.37 (s, 2H), 3.99 (d, *J* = 12.7 Hz, 2H), 3.21 (s, 3H), 3.08–2.65 (m, 3H), 1.88 (d, *J* = 11.0 Hz, 2H), 1.70–1.45 (m, 2H), 1.40 (s, 9H); HRMS (ESI) calcd for C₂₂H₂₉N₃O₅S (M – ^tBu + H)⁺ 392.1275, found 392.1273.

tert-Butyl (3S)-3-Methyl-4-(5-[[4-(methylsulfonyl)benzyl]oxy]pyrimidin-2-yl)piperazine-1-carboxylate (11). Compound 11 was synthesized as described for 2 using (*S*)-*tert*-butyl 4-(5-hydroxypyrimidin-2-yl)-3-methylpiperazine-1-carboxylate in 94% yield: ¹H NMR (400 MHz, CDCl₃) δ 8.05 (s, 2H), 7.90 (d, *J* = 8.4 Hz, 2H), 7.55 (d, *J* = 8.5 Hz, 2H), 5.04 (s, 2H), 4.77–4.61 (m, 1H), 4.24 (d, *J* = 13.3 Hz, 1H), 4.16–3.72 (m, 2H), 3.08 (ddd, *J* = 13.3, 12.1, 3.6 Hz, 1H), 2.99 (s, 3H), 2.94–2.78 (m, 2H), 1.42 (s, 9H), 1.08

(d, $J = 6.7$ Hz, 3H); HRMS (ESI) calcd for $C_{22}H_{31}O_5N_4S$ ($M + H$)⁺ 463.2010, found 463.2011.

tert-Butyl (3R)-3-Methyl-4-(5-[[4-(methylsulfonyl)benzyl]oxy]pyrimidin-2-yl)piperazine-1-carboxylate (12). To a stirred solution of (*R*)-*tert*-butyl 4-(5-hydroxypyrimidin-2-yl)-3-methylpiperazine-1-carboxylate (5.0 g, 16.99 mmol), and 1-(chloromethyl)-4-(methylsulfonyl)benzene (3.65 g, 17.84 mmol) in acetonitrile (170 mL) at ambient temperature was added potassium carbonate (7.04 g, 50.96 mmol). The mixture was heated under reflux at 80 °C for 2 h and cooled to ambient temperature, and the acetonitrile was evaporated in vacuo to give a residue which was partitioned between ethyl acetate (160 mL) and water (80 mL). The ethyl acetate layer was washed with brine, dried (MgSO₄), and evaporated in vacuo to a residue which was crystallized from ethyl acetate/isohexane to give *tert*-butyl (3R)-3-methyl-4-(5-[[4-(methylsulfonyl)benzyl]oxy]pyrimidin-2-yl)piperazine-1-carboxylate (7.25 g, 92%): mp 173–174 °C; ¹H NMR (400 MHz, DMSO, 100 °C) δ 8.26 (s, 2H), 7.94 (d, $J = 8.4$ Hz, 2H), 7.69 (d, $J = 8.4$ Hz, 2H), 5.22 (s, 2H), 4.81–4.61 (m, 1H), 4.25 (dt, $J = 13.4, 3.2$ Hz, 1H), 3.99–3.88 (m, 1H), 3.79 (dt, $J = 13.2, 2.0$ Hz, 1H), 3.17 (s, 3H), 3.15–3.05 (m, 2H), 2.94–2.87 (m, 1H), 1.44 (s, 9H), 1.08 (d, $J = 6.6$ Hz, 3H); HRMS (ESI) calcd for $C_{22}H_{31}O_5N_4S$ ($M + H$)⁺ 463.2010, found 463.2009.

tert-Butyl (2R)-2-Methyl-4-(5-[[4-(methylsulfonyl)benzyl]oxy]pyrimidin-2-yl)piperazine-1-carboxylate (13). Compound 13 was synthesized as described for 2 using (*R*)-*tert*-butyl 4-(5-hydroxypyrimidin-2-yl)-2-methylpiperazine-1-carboxylate as the starting material in 40% yield: mp 145–146 °C; ¹H NMR (400 MHz, CDCl₃) δ 8.11 (s, 2H), 7.97 (d, $J = 8.4$ Hz, 2H), 7.62 (d, $J = 8.6$ Hz, 2H), 5.11 (s, 2H), 4.48–4.39 (m, 1H), 4.40–4.27 (m, 2H), 3.95–3.86 (m, 1H), 3.22–3.09 (m, 2H), 3.06 (s, 3H), 2.97 (td, $J = 12.1, 3.7$ Hz, 1H), 1.48 (s, 9H), 1.15 (d, $J = 6.7$ Hz, 3H); HRMS (ESI) calcd for $C_{22}H_{31}O_5N_4S$ ($M + H$)⁺ 463.2009, found 463.2008.

tert-Butyl (2S)-2-Methyl-4-(5-[[4-(methylsulfonyl)benzyl]oxy]pyrimidin-2-yl)piperazine-1-carboxylate (14). Compound 14 was synthesized as described for 2 using (*S*)-*tert*-butyl 4-(5-hydroxypyrimidin-2-yl)-2-methylpiperazine-1-carboxylate as the starting material in 29% yield: ¹H NMR (400 MHz, CDCl₃) δ 8.11 (s, 2H), 8.00–7.95 (m, 2H), 7.64–7.59 (m, 2H), 5.11 (s, 2H), 4.48–4.41 (m, 1H), 4.39–4.26 (m, 2H), 3.94–3.86 (m, 1H), 3.20–3.11 (m, 2H), 3.06 (s, 3H), 3.01–2.93 (m, 1H), 1.48 (s, 9H), 1.15 (d, $J = 6.7$ Hz, 3H); HRMS (ESI) calcd for $C_{22}H_{31}O_5N_4S$ ($M + H$)⁺ 463.2010, found 463.2007.

tert-Butyl 3,3-Dimethyl-4-(5-[[4-(methylsulfonyl)benzyl]oxy]pyrimidin-2-yl)piperazine-1-carboxylate (15). Compound 15 was synthesized as described for 2 using *tert*-butyl 4-(5-hydroxypyrimidin-2-yl)-3,3-dimethylpiperazine-1-carboxylate as the starting material in 28% yield: mp 140–141 °C; ¹H NMR (400 MHz, CDCl₃) δ 8.11 (s, 2H), 8.01–7.94 (m, 2H), 7.62 (d, $J = 8.5$ Hz, 2H), 5.11 (s, 2H), 4.04–3.94 (m, 2H), 3.62–3.41 (m, 4H), 3.06 (s, 3H), 1.51 (s, 6H), 1.48 (s, 9H); HRMS (ESI) calcd for $C_{23}H_{33}O_5N_4S$ ($M + H$)⁺ 477.2166, found 477.2161.

tert-Butyl (3R,5S)-3,5-Dimethyl-4-(5-[[4-(methylsulfonyl)benzyl]oxy]pyrimidin-2-yl)piperazine-1-carboxylate (16). Compound 16 was synthesized as described for 2 using *tert*-butyl (3R,5S)-4-(5-hydroxypyrimidin-2-yl)-3,5-dimethylpiperazine-1-carboxylate as the starting material in 25% yield: ¹H NMR (400 MHz, CDCl₃) δ 8.15 (s, 2H), 8.01–7.94 (m, 2H), 7.62 (d, $J = 8.5$ Hz, 2H), 5.11 (s, 2H), 4.66 (s, 3H), 4.22–3.82 (m, 3H), 3.06 (s, 3H), 1.50 (s, 9H), 1.23 (s, 3H), 1.21 (s, 3H); HRMS (ESI) calcd for $C_{23}H_{33}O_5N_4S$ ($M + H$)⁺ 477.2166, found 477.2164.

tert-Butyl (2R,5S)-2,5-Dimethyl-4-(5-[[4-(methylsulfonyl)benzyl]oxy]pyrimidin-2-yl)piperazine-1-carboxylate (17). Compound 17 was synthesized as described for 2 using *tert*-butyl (2R,5S)-4-(5-hydroxypyrimidin-2-yl)-2,5-dimethylpiperazine-1-carboxylate as the starting material in 30% yield: ¹H NMR (400 MHz, CDCl₃) δ 8.11 (s, 2H), 8.00–7.95 (m, 2H), 7.62 (d, $J = 8.5$ Hz, 2H), 5.11 (s, 2H), 4.84–4.70 (m, 1H), 4.48 (s, 1H), 4.32–4.15 (m, 1H), 3.86–3.67 (m, 1H), 3.36–3.23 (m, 2H), 3.06 (s, 3H), 1.48 (s, 9H), 1.15 (d, $J = 5.6$ Hz, 6H); HRMS (ESI) calcd for $C_{23}H_{33}O_5N_4S$ ($M + H$)⁺ 477.2166, found 477.2163.

tert-Butyl (1R,4R)-5-(5-[[4-(Methylsulfonyl)benzyl]oxy]pyrimidin-2-yl)-2,5-diazabicyclo[2.2.1]heptane-2-carboxylate (18). Compound 18 was synthesized as described for 2 using *tert*-butyl (1R,4R)-5-(5-hydroxypyrimidin-2-yl)-2,5-diazabicyclo[2.2.1]heptane-2-carboxylate in 59% yield: mp 202–203 °C; ¹H NMR (400 MHz, DMSO) δ 8.23 (s, 2H), 7.94 (d, $J = 8.3$ Hz, 2H), 7.69 (d, $J = 8.3$ Hz, 2H), 5.20 (s, 2H), 4.81 (s, 1H), 4.45 (s, 1H), 3.49 (dd, $J = 10.2, 1.8$ Hz, 1H), 3.44–3.32 (m, 2H), 3.16 (s, 4H), 1.88 (s, 2H), 1.39 (s, 9H); HRMS (ESI) calcd for $C_{22}H_{28}O_5N_4S$ ($M + H$)⁺ 461.1853, found 461.1854.

tert-Butyl (1R,4S)-5-(5-[[4-(Methylsulfonyl)benzyl]oxy]pyrimidin-2-yl)-2,5-diazabicyclo[2.2.2]octane-2-carboxylate (19). Compound 19 was synthesized as described for 2 using *tert*-butyl (1S,4S)-5-(5-hydroxypyrimidin-2-yl)-2,5-diazabicyclo[2.2.2]octane-2-carboxylate in 48% yield: mp 154–155 °C; ¹H NMR (400 MHz, CDCl₃) δ 8.04 (s, 2H), 7.90 (d, $J = 8.4$ Hz, 2H), 7.55 (d, $J = 8.2$ Hz, 2H), 5.03 (s, 2H), 4.86–4.73 (m, 1H), 4.40–4.14 (m, 1H), 3.77–3.63 (m, 1H), 3.61–3.35 (m, 3H), 2.99 (s, 3H), 2.08–1.85 (m, 2H), 1.85–1.63 (m, 2H), 1.30 (s, 9H); HRMS (ESI) calcd for $C_{23}H_{31}O_5N_4S$ ($M + H$)⁺ 475.2010, found 475.2006.

tert-Butyl (3R)-3-Methyl-4-(5-[[1-(methylsulfonyl)piperidin-4-yl]methoxy]pyrimidin-2-yl)piperazine-1-carboxylate (20). To a stirred solution of (*R*)-*tert*-butyl 4-(5-hydroxypyrimidin-2-yl)-3-methylpiperazine-1-carboxylate (8.83 g, 30.0 mmol) and 1-(methylsulfonyl)piperidin-4-yl)methyl methanesulfonate (8.95 g, 33.0 mmol) in DMF (150 mL) was added cesium carbonate (19.55 g, 60.00 mmol), and the mixture was heated at 55 °C for 16 h. The mixture was cooled to ambient temperature, the dimethylformamide evaporated in vacuo to a residue which was partitioned between water (270 mL) and ethyl acetate (450 mL), and the ethyl acetate layer washed with brine, dried (MgSO₄), and evaporated in vacuo to a residue which was crystallized from ethyl acetate/isohexane to give *tert*-butyl (3R)-3-methyl-4-(5-[[1-(methylsulfonyl)piperidin-4-yl]methoxy]pyrimidin-2-yl)piperazine-1-carboxylate (9.88 g, 70%). The mother liquors from the crystallization were evaporated in vacuo to a residue which was chromatographed on silica with 50% ethyl acetate in isohexane as the eluant to give a solid which was crystallized from ethyl acetate/isohexane to give a further 2.1 g of product, giving a total yield of 85%: mp 162–164 °C; ¹H NMR (400 MHz, DMSO, 100 °C) δ 8.19 (s, 2H), 4.77–4.63 (m, 1H), 4.24 (dt, $J = 13.3, 3.2$ Hz, 1H), 3.89 (d, $J = 6.0$ Hz, 2H), 3.79 (dt, $J = 13.2, 1.9$ Hz, 1H), 3.62 (d, $J = 12.1$ Hz, 2H), 3.20–3.02 (m, 2H), 2.95 (s, 3H), 2.95–2.87 (m, 2H), 2.77 (d, $J = 2.5$ Hz, 1H), 1.87 (m, 4H), 1.49–1.44 (m, 2H), 1.44 (s, 9H), 1.08 (d, $J = 6.6$ Hz, 3H); HRMS (ESI) calcd for $C_{21}H_{36}O_5N_5S$ ($M + H$)⁺ 470.2432, found 470.2429.

tert-Butyl (3R)-4-(5-[[4-(Dimethylsulfamoyl)benzyl]oxy]pyrimidin-2-yl)-3-methylpiperazine-1-carboxylate (21). Compound 21 was synthesized as described for 20 using (*R*)-*tert*-butyl 4-(5-((4-bromo-2-cyanobenzyl)oxy)pyrimidin-2-yl)-3-methylpiperazine-1-carboxylate and 4-(*N,N*-dimethylsulfamoyl)benzyl methanesulfonate as starting materials in 91% yield: ¹H NMR (400 MHz, DMSO, 100 °C) δ 8.26 (s, 2H), 7.78–7.75 (m, 2H), 7.71–7.66 (m, 2H), 5.20 (s, 2H), 4.76–4.66 (m, 1H), 4.32–4.20 (m, 1H), 3.98–3.88 (m, 1H), 3.84–3.74 (m, 1H), 3.20–3.06 (m, 2H), 2.98–2.86 (m, 1H), 2.67 (s, 6H), 1.44 (s, 9H), 1.08 (d, $J = 6.6$ Hz, 3H); HRMS (ESI) calcd for $C_{23}H_{34}O_5N_5S$ ($M + H$)⁺ 492.2275, found 492.2274.

tert-Butyl (3R)-4-(5-[[4-(Cyanobenzyl)oxy]pyrimidin-2-yl]-3-methylpiperazine-1-carboxylate (22). To a mixture of (*R*)-*tert*-butyl 4-(5-hydroxypyrimidin-2-yl)-3-methylpiperazine-1-carboxylate (295 mg, 1.00 mmol), 4-(bromomethyl)benzotrile (216 mg, 1.10 mmol), and cesium carbonate (980 mg, 3.01 mmol) under an atmosphere of nitrogen in a microwave vial was added acetonitrile (13.5 mL). The mixture was heated at 100 °C for 1 h, and the acetonitrile was evaporated in vacuo to a residue which was taken up in ethyl acetate (50 mL), washed with water and brine, dried (MgSO₄), and evaporated in vacuo to a residue which was chromatographed on silica with 30% ethyl acetate in isohexane as the eluant to give a solid which was crystallized from ethyl acetate/isohexane to give *tert*-butyl (3R)-4-(5-[[4-(cyanobenzyl)oxy]pyrimidin-2-yl]-3-methylpiperazine-1-carboxylate (343 mg, 84%): mp 144–145 °C; ¹H NMR (400 MHz,

DMSO, 100 °C) δ 8.24 (s, 2H), 7.81 (d, J = 8.4 Hz, 2H), 7.62 (d, J = 8.0 Hz, 2H), 5.19 (s, 2H), 4.76–4.62 (m, 1H), 4.24 (d, J = 13.4 Hz, 1H), 3.97–3.87 (m, 1H), 3.83–3.73 (m, 1H), 3.19–3.04 (m, 3H), 2.98–2.89 (m, 1H), 1.43 (s, 9H), 1.08 (d, J = 6.6 Hz, 3H); HRMS (ESI) calcd for $C_{22}H_{28}O_3N_5$ ($M + H$)⁺ 410.2187, found 410.2187.

tert-Butyl (3R)-3-Methyl-4-(5-[[4-(1H-tetrazol-1-yl)benzyl]oxy]pyrimidin-2-yl)piperazine-1-carboxylate (23). Diisopropyl azodicarboxylate (0.176 mL, 0.89 mmol) was added to a stirred solution of (*R*)-*tert*-butyl 4-(5-hydroxypyrimidin-2-yl)-3-methylpiperazine-1-carboxylate (0.21 g, 0.71 mmol), and triphenylphosphine (0.281 g, 1.07 mmol) in THF (15 mL) under nitrogen. The resulting solution was stirred at 20 °C for 30 min, and then (4-(1H-tetrazol-1-yl)phenyl)methanol (0.157 g, 0.89 mmol) was added. The resulting solution was stirred at room temperature overnight under nitrogen. The solvent was evaporated and the residue diluted with EtOAc and brine. A white precipitate was filtered off and dried under vacuum. The aqueous layer was extracted with EtOAc (50 mL), and the combined organics were concentrated in vacuo to afford crude product. The crude product was purified by flash silica chromatography, elution gradient 1–4% MeOH in CH_2Cl_2 . The crude product was repurified by flash silica chromatography, elution gradient 40–100% EtOAc in isohexane. Pure fractions were evaporated to dryness to afford *tert*-butyl (3R)-3-methyl-4-(5-[[4-(1H-tetrazol-1-yl)benzyl]oxy]pyrimidin-2-yl)piperazine-1-carboxylate (87 mg, 27%) as a white solid: mp 202–203 °C; ¹H NMR (400 MHz, $CDCl_3$) δ 8.99 (s, 1H), 8.14 (s, 2H), 7.80–7.22 (m, 2H), 7.68–7.60 (m, 2H), 5.11 (s, 2H), 4.84–4.69 (m, 1H), 4.32 (d, J = 13.1 Hz, 1H), 4.13 (s, 2H), 3.20–3.03 (m, 2H), 3.01–2.76 (m, 1H), 1.49 (s, 9H), 1.15 (d, J = 6.7 Hz, 3H); HRMS (ESI) calcd for $C_{22}H_{29}O_3N_8$ ($M + H$)⁺ 453.2357, found 453.2358.

tert-Butyl (3R)-4-(5-[[2-Fluoro-4-(methylsulfonyl)benzyl]oxy]pyrimidin-2-yl)-3-methylpiperazine-1-carboxylate (24). Copper(I) iodide (2.58 μ L, 0.07 mmol) was added to (*R*)-*tert*-butyl 4-(5-((4-bromo-2-fluorobenzyl)oxy)pyrimidin-2-yl)-3-methylpiperazine-1-carboxylate (330 mg, 0.69 mmol), methanesulfonic acid sodium salt (84 mg, 0.82 mmol), L-proline (15.79 mg, 0.14 mmol), and sodium hydroxide (4.06 μ L, 0.14 mmol) in DMSO (3.0 mL) under nitrogen. The resulting solution was degassed with nitrogen for 20 min and stirred at 80 °C for 2 d. It was cooled to room temperature and partitioned between 50% brine (50 mL) and ethyl acetate (150 mL). The aqueous portion was extracted with ethyl acetate (2 \times 100 mL), and all of the combined organics were washed with brine (50 mL), dried (sodium sulfate), concentrated in vacuo, and adsorbed onto silica. The crude product was purified by flash silica chromatography, elution gradient 0–75% EtOAc in isohexane. Pure fractions were evaporated to dryness to afford *tert*-butyl (3R)-4-(5-[[2-fluoro-4-(methylsulfonyl)benzyl]oxy]pyrimidin-2-yl)-3-methylpiperazine-1-carboxylate (190 mg, 58%) as a white solid: mp 124–125 °C; ¹H NMR (400 MHz, DMSO) δ 8.31 (s, 2H), 7.93–7.74 (m, 3H), 5.25 (s, 2H), 4.77–4.57 (m, 1H), 4.23 (d, J = 13.0 Hz, 1H), 3.94 (s, 1H), 3.80 (d, J = 13.1 Hz, 1H), 3.27 (s, 3H), 3.14–2.96 (m, 2H), 2.86 (s, 1H), 1.41 (s, 9H), 1.03 (d, J = 6.6 Hz, 3H); HRMS (ESI) calcd for $C_{22}H_{29}O_5N_4SF$ ($M + H$)⁺ 481.1916, found 481.1912.

tert-Butyl (3R)-4-(5-[[2-Cyano-4-(methylsulfonyl)benzyl]oxy]pyrimidin-2-yl)-3-methylpiperazine-1-carboxylate (25). Compound 25 was synthesized as described for 24 using (*R*)-*tert*-butyl 4-(5-((4-bromo-2-cyanobenzyl)oxy)pyrimidin-2-yl)-3-methylpiperazine-1-carboxylate as the starting material in 50% yield: mp 159–160 °C; ¹H NMR (400 MHz, DMSO, 100 °C) δ 8.39 (d, J = 1.8 Hz, 1H), 8.30 (s, 2H), 8.25 (dd, J = 8.2, 1.9 Hz, 1H), 7.98 (d, J = 8.2 Hz, 1H), 5.35 (s, 2H), 4.78–4.67 (m, 1H), 4.27 (dt, J = 13.4, 3.3 Hz, 1H), 3.93 (d, J = 12.9 Hz, 1H), 3.80 (dt, J = 13.2, 1.8 Hz, 1H), 3.13 (ddd, J = 13.4, 12.3, 3.7 Hz, 2H), 2.95 (s, 3H), 3.01–2.90 (m, 1H), 1.44 (s, 9H), 1.10 (d, J = 6.6 Hz, 3H); HRMS (ESI) calcd for $C_{23}H_{30}O_5N_5S$ ($M + H$)⁺ 488.1962, found 488.1960.

tert-Butyl (3R)-3-Methyl-4-(5-[[5-(methylsulfonyl)pyridin-2-yl]methoxy]pyrimidin-2-yl)piperazine-1-carboxylate (26). Compound 26 was synthesized as described for 24 using (*R*)-*tert*-butyl 4-(5-((5-bromopyridin-2-yl)methoxy)pyrimidin-2-yl)-3-methylpiperazine-1-carboxylate as the starting material in 26% yield: mp 219–220 °C; ¹H NMR (400 MHz, $CDCl_3$) δ 9.12 (d, J = 2.3 Hz, 1H),

8.27 (dd, J = 2.3, 8.2 Hz, 1H), 8.17 (s, 2H), 7.76 (d, J = 8.2 Hz, 1H), 5.24 (s, 2H), 4.84–4.71 (m, 1H), 4.32 (d, J = 10.8 Hz, 1H), 4.23–3.82 (m, 2H), 3.22–3.14 (m, 2H), 3.12 (s, 3H), 3.01–2.77 (m, 1H), 1.49 (s, 9H), 1.15 (d, J = 6.7 Hz, 3H); HRMS (ESI) calcd for $C_{21}H_{30}O_5N_5S$ ($M + H$)⁺ 464.1962, found 464.1962.

tert-Butyl 4-[5-(Pyridin-4-ylmethoxy)pyrimidin-2-yl]piperazine-1-carboxylate (27). Compound 27 was synthesized as described for 22 using *tert*-butyl 4-(5-hydroxypyrimidin-2-yl)piperazine-1-carboxylate and 4-(bromomethyl)nicotinonitrile as starting materials in 32% yield: mp 147–148 °C; ¹H NMR (400 MHz, $CDCl_3$) δ 8.68–8.58 (m, 2H), 8.12 (s, 2H), 7.37–7.29 (m, 2H), 5.04 (s, 2H), 3.71 (dd, J = 6.2, 4.3 Hz, 4H), 3.52–3.46 (m, 4H), 1.48 (s, 9H); HRMS (ESI) calcd for $C_{19}H_{26}O_3N_5$ ($M + H$)⁺ 372.2030, found 372.2029.

tert-Butyl 4-[5-[(2-Methylpyridin-4-yl)methoxy]pyrimidin-2-yl]piperazine-1-carboxylate (28). Cesium carbonate (2.111 g, 6.48 mmol) was added to a mixture of 4-(chloromethyl)-2-methylpyridine hydrochloride (0.288 g, 1.62 mmol) and *tert*-butyl 4-(5-hydroxypyrimidin-2-yl)piperazine-1-carboxylate (0.454 g, 1.62 mmol) in DMF (5 mL). The resulting mixture was stirred at 40 °C for 2 h. The reaction mixture was diluted with EtOAc (75 mL) and washed sequentially with water (20 mL) and saturated brine (20 mL). The organic layer was dried over Na_2SO_4 , filtered, and evaporated to afford crude product. The crude product was purified by flash alumina chromatography, elution gradient 0–70% EtOAc in isohexane. Pure fractions were evaporated to dryness to afford *tert*-butyl 4-[5-[(2-methylpyridin-4-yl)methoxy]pyrimidin-2-yl]piperazine-1-carboxylate (194 mg, 31%) as a yellow solid: mp 97–98 °C; ¹H NMR (400 MHz, DMSO) δ 8.49 (d, J = 5.06 Hz, 1H), 8.34 (s, 2H), 7.36–7.33 (m, 1H), 7.29–7.25 (m, 1H), 5.19 (s, 2H), 3.71–3.63 (m, 4H), 3.47–3.40 (m, 4H), 1.48 (s, 9H); HRMS (ESI) calcd for $C_{20}H_{28}O_3N_5$ ($M + H$)⁺ 386.2187, found 386.2185.

tert-Butyl 4-[5-[(3-Methylpyridin-4-yl)methoxy]pyrimidin-2-yl]piperazine-1-carboxylate (29). Compound 29 was synthesized as described for 23 using *tert*-butyl 4-(5-hydroxypyrimidin-2-yl)piperazine-1-carboxylate and (3-methylpyridin-4-yl)methanol as starting materials in 61% yield: mp 154–155 °C; ¹H NMR (400 MHz, DMSO) δ 8.40 (d, J = 5.1 Hz, 2H), 8.31 (s, 2H), 7.39 (d, J = 4.9 Hz, 1H), 5.15 (s, 2H), 3.74–3.52 (m, 4H), 3.45–3.32 (m, 4H), 2.28 (s, 3H), 1.41 (s, 9H); HRMS (ESI) calcd for $C_{20}H_{27}O_3N_5$ ($M + H$)⁺ 386.2187, found 386.2185.

tert-Butyl 4-[5-[(3-Methoxypyridin-4-yl)methoxy]pyrimidin-2-yl]piperazine-1-carboxylate (30). Compound 30 was synthesized as described for 23 using *tert*-butyl 4-(5-hydroxypyrimidin-2-yl)piperazine-1-carboxylate and (3-methoxypyridin-4-yl)methanol as starting materials in 37% yield: mp 126–127 °C; ¹H NMR (400 MHz, DMSO) δ 8.38 (s, 1H), 8.27 (s, 2H), 8.23 (d, J = 4.7 Hz, 1H), 7.41 (d, J = 4.7 Hz, 1H), 5.11 (s, 2H), 3.93 (s, 3H), 3.61 (dd, J = 6.2, 4.3 Hz, 4H), 3.40–3.35 (m, 4H), 1.41 (s, 9H); HRMS (ESI) calcd for $C_{20}H_{27}O_4N_5$ ($M + H$)⁺ 402.2136, found 402.2135.

tert-Butyl 4-[5-[(3-Fluoropyridin-4-yl)methoxy]pyrimidin-2-yl]piperazine-1-carboxylate (31). Compound 31 was synthesized as described for 23 using *tert*-butyl 4-(5-hydroxypyrimidin-2-yl)piperazine-1-carboxylate and (3-fluoropyridin-4-yl)methanol as starting materials in 46% yield: mp 148–148 °C; ¹H NMR (400 MHz, $CDCl_3$) δ 8.46 (s, 1H), 8.41–8.37 (m, 1H), 8.09 (s, 2H), 7.43 (m, 1H), 5.06 (s, 2H), 3.68 (dd, J = 6.2, 4.3 Hz, 4H), 3.43 (dd, J = 6.2, 4.3 Hz, 4H), 1.41 (s, 9H); HRMS (ESI) calcd for $C_{19}H_{25}O_3N_5F$ ($M + H$)⁺ 390.1935, found 390.1936.

tert-Butyl 4-[5-[(3-Cyanopyridin-4-yl)methoxy]pyrimidin-2-yl]piperazine-1-carboxylate (32). *tert*-Butyl 4-(5-((3-bromopyridin-4-yl)methoxy)pyrimidin-2-yl)piperazine-1-carboxylate (0.95 g, 2.11 mmol), zinc cyanide (0.198 g, 1.69 mmol), tris(dibenzylideneacetone)dipalladium(0) (0.077 g, 0.08 mmol), and 4,5-bis(diphenylphosphino)-9,9-dimethylxanthene (xantphos; 0.098 g, 0.17 mmol) were suspended in DMF (20 mL) and sealed into a microwave tube (evacuated and purged with nitrogen). The reaction was heated to 130 °C for 60 min in the microwave reactor and cooled to room temperature. The reaction mixture was filtered through Celite. The reaction mixture was diluted with EtOAc (100 mL) and washed

sequentially with water (100 mL) and saturated brine (100 mL). The organic layer was dried over Na_2SO_4 , filtered, and evaporated to afford crude product that was purified by flash silica chromatography, elution gradient 1–4% MeOH in CH_2Cl_2 and by flash silica chromatography, elution gradient 20–80% EtOAc in isohexane. Pure fractions were evaporated to dryness to afford *tert*-butyl 4- $\{5-[(3\text{-cyanopyridin-4-yl)methoxy]pyrimidin-2-yl\}$ piperazine-1-carboxylate (410 mg, 49%) as a white solid: mp 107–108 °C; ^1H NMR (400 MHz, CDCl_3) δ 8.90 (s, 1H), 8.84 (d, $J = 5.2$ Hz, 1H), 8.17 (s, 2H), 7.65 (d, $J = 5.2$ Hz, 1H), 5.21 (s, 2H), 3.80–3.70 (m, 4H), 3.54–3.45 (m, 4H), 1.49 (s, 9H); HRMS (ESI) calcd for $\text{C}_{20}\text{H}_{25}\text{O}_3\text{N}_6$ ($M + \text{H}$) $^+$ 397.1983, found 397.1981.

***tert*-Butyl 4- $\{5-[(3\text{-Methylsulfonyl)pyridin-4-yl}]\text{methoxy}]\text{pyrimidin-2-yl}\}$ piperazine-1-carboxylate (33).** Compound 33 was synthesized as described for 24 using *tert*-butyl 4- $\{5-[(3\text{-bromopyridin-4-yl)methoxy}]\text{pyrimidin-2-yl}\}$ piperazine-1-carboxylate as the starting material in 33% yield: mp 148–149 °C; ^1H NMR (400 MHz, CDCl_3) δ 9.14 (s, 1H), 8.84 (d, $J = 5.1$ Hz, 1H), 8.12 (s, 2H), 7.76–7.58 (m, 2H), 5.06 (s, 2H), 5.37 (s, 2H), 3.67 (dd, $J = 6.2$, 4.3 Hz, 4H), 3.43 (dd, $J = 6.2$, 4.3 Hz, 4H), 3.11 (s, 3H), 1.42 (s, 9H); HRMS (ESI) calcd for $\text{C}_{20}\text{H}_{28}\text{O}_3\text{N}_5\text{S}$ ($M + \text{H}$) $^+$ 450.1806, found 450.1803.

***tert*-Butyl 4- $\{5-[(3,5\text{-Difluoropyridin-4-yl})\text{methoxy}]\text{pyrimidin-2-yl}\}$ piperazine-1-carboxylate (34).** Compound 34 was synthesized as described for 23 using *tert*-butyl 4- $\{5\text{-hydroxypyrimidin-2-yl}\}$ piperazine-1-carboxylate and $(3,5\text{-difluoropyridin-4-yl})\text{-methanol}$ as starting materials in 50% yield: ^1H NMR (400 MHz, CDCl_3) δ 8.41 (s, 1H), 8.14 (s, 1H), 7.26 (s, 1H), 5.13 (s, 2H), 3.78–3.68 (m, 4H), 3.53–3.44 (m, 4H), 1.48 (s, 9H); HRMS (ESI) calcd for $\text{C}_{19}\text{H}_{24}\text{O}_3\text{N}_5\text{F}_2$ ($M + \text{H}$) $^+$ 408.1842, found 408.1840.

***tert*-Butyl (3*R*)-3-Methyl-4- $\{5\text{-[pyridin-4-yl]methoxy}\}$ pyrimidin-2-yl]piperazine-1-carboxylate (35).** Compound 35 was synthesized as described for 28 using (*R*)-*tert*-butyl 4- $\{5\text{-hydroxypyrimidin-2-yl}\}$ -3-methylpiperazine-1-carboxylate and 3-methyl-4-(chloromethyl)pyridine hydrochloride as starting materials in 51% yield: mp 126–128 °C; ^1H NMR (400 MHz, DMSO, 100 °C) δ 8.57 (d, $J = 6.0$ Hz, 2H), 8.25 (s, 2H), 7.40 (d, $J = 5.9$ Hz, 2H), 5.14 (s, 2H), 4.70 (ddd, $J = 6.5$, 3.9, 2.5 Hz, 1H), 4.25 (dt, $J = 13.4$, 3.2 Hz, 1H), 3.92 (dt, $J = 12.9$, 3.9 Hz, 1H), 3.79 (dt, $J = 13.2$, 1.0 Hz, 1H), 3.16–3.05 (m, 2H), 2.99–2.85 (m, 1H), 1.44 (s, 9H), 1.08 (d, $J = 6.6$ Hz, 3H); HRMS (ESI) calcd for $\text{C}_{20}\text{H}_{28}\text{O}_3\text{N}_5$ ($M + \text{H}$) $^+$ 386.2187, found 386.2187.

***tert*-Butyl (3*R*)-4- $\{5-[(3\text{-Cyanopyridin-4-yl})\text{methoxy}]\text{pyrimidin-2-yl}\}$ -3-methylpiperazine-1-carboxylate (36).** Compound 36 was synthesized as described for 32 using (*R*)-*tert*-butyl 4- $\{5-[(3\text{-bromopyridin-4-yl})\text{methoxy}]\text{pyrimidin-2-yl}\}$ -3-methylpiperazine-1-carboxylate as the starting material in 93% yield: mp 91–93 °C; ^1H NMR (400 MHz, CDCl_3) δ 8.93–8.88 (m, 1H), 8.84 (d, $J = 5.2$ Hz, 1H), 8.18 (s, 2H), 7.66 (dd, $J = 5.2$, 0.8 Hz, 1H), 5.25–5.18 (m, 2H), 4.85–4.68 (m, 1H), 4.34 (d, $J = 13.3$ Hz, 1H), 4.22–3.84 (m, 2H), 3.21–3.05 (m, 2H), 3.01–2.74 (m, 1H), 1.49 (s, 9H), 1.16 (d, $J = 6.7$ Hz, 3H); HRMS (ESI) calcd for $\text{C}_{21}\text{H}_{27}\text{O}_3\text{N}_6$ ($M + \text{H}$) $^+$ 411.2139, found 411.2138.

1-Methylethyl (3*R*)-4- $\{5-[(3\text{-Cyanopyridin-4-yl})\text{methoxy}]\text{pyrimidin-2-yl}\}$ -3-methylpiperazine-1-carboxylate (37). To a stirred solution of (*R*)-4- $\{[(2\text{-methylpiperazin-1-yl})\text{pyrimidin-5-yloxy}]\text{methyl}\}$ nicotinonitrile (320 mg, 1.03 mmol) and *N,N*-diisopropylethylamine (0.360 mL, 2.06 mmol) in dichloromethane (37 mL) under nitrogen at 0 °C was added isopropyl chloroformate (1.24 mL, 1.24 mmol). The mixture was stirred at 0 °C for 1 h and then at ambient temperature for 16 h. The dichloromethane was evaporated in vacuo to a residue which was taken up in ethyl acetate (50 mL), washed with 2 M sodium carbonate solution and brine, dried (MgSO_4), and evaporated in vacuo to a residue which was chromatographed on silica with 50–100% ethyl acetate in isohexane as the eluant to give 1-methylethyl (3*R*)-4- $\{5-[(3\text{-cyanopyridin-4-yl})\text{methoxy}]\text{pyrimidin-2-yl}\}$ -3-methylpiperazine-1-carboxylate (165 mg, 40%): ^1H NMR (400 MHz, CDCl_3) δ 8.84 (s, 1H), 8.78 (d, $J = 5.2$ Hz, 1H), 8.11 (s, 2H), 7.59 (d, $J = 5.2$ Hz, 1H), 5.14 (s, 2H), 4.90 (hept, $J = 6.2$ Hz, 1H), 4.79–4.65 (m, 1H), 4.29 (d, $J = 12.9$ Hz,

1H), 4.22–3.80 (m, 2H), 3.18–2.99 (m, 2H), 2.97–2.79 (m, 1H), 1.20 (d, $J = 6.2$ Hz, 6H), 1.09 (d, $J = 6.7$ Hz, 3H); HRMS (ESI) calcd for $\text{C}_{20}\text{H}_{25}\text{O}_3\text{N}_6$ ($M + \text{H}$) $^+$ 397.1983, found 397.1981.

1-Cyano-1-methylethyl (3*R*)-4- $\{5-[(3\text{-Cyanopyridin-4-yl})\text{methoxy}]\text{pyrimidin-2-yl}\}$ -3-methylpiperazine-1-carboxylate (38). Triethylamine (0.251 mL, 1.80 mmol) was added to (*R*)-4- $\{[(2\text{-methylpiperazin-1-yl})\text{pyrimidin-5-yloxy}]\text{methyl}\}$ nicotinonitrile (0.28 g, 0.90 mmol) and 2-cyanopropan-2-yl phenyl carbonate (0.278 g, 1.35 mmol) in chloroform (2 mL) under nitrogen. The resulting solution was stirred at 110 °C for 18 h, during which time all the solvent was evaporated to leave a thick gum. The reaction mixture was diluted with CH_2Cl_2 (50 mL) and washed with 2 M K_2CO_3 aq. (20 mL). The organic layer was dried over Na_2SO_4 , filtered, and evaporated to afford crude product that was purified by flash silica chromatography, elution gradient 0–5% MeOH in CH_2Cl_2 . The crude solid was triturated with Et_2O and then crystallized from hot EtOH to give 1-cyano-1-methylethyl (3*R*)-4- $\{5-[(3\text{-cyanopyridin-4-yl})\text{methoxy}]\text{pyrimidin-2-yl}\}$ -3-methylpiperazine-1-carboxylate (62 mg, 16%) as a white solid: ^1H NMR (400 MHz, CDCl_3) δ 8.91 (s, 1H), 8.85 (d, $J = 5.2$ Hz, 1H), 8.19 (s, 2H), 7.71–7.62 (m, 1H), 5.21 (s, 2H), 4.89–4.75 (m, 1H), 4.46–4.34 (d, $J = 13.5$ Hz, 1H), 4.05–3.89 (m, 1H), 3.80 (d, $J = 13.4$ Hz, 1H), 3.20 (td, $J = 13.3$, 3.5 Hz, 2H), 3.12–2.92 (m, 1H), 1.80 (s, 6H), 1.18 (d, $J = 6.1$ Hz, 3H); HRMS (ESI) calcd for $\text{C}_{21}\text{H}_{24}\text{O}_3\text{N}_7$ ($M + \text{H}$) $^+$ 422.1935, found 422.1932.

2,2,2-Trifluoroethyl (3*R*)-4- $\{5-[(3\text{-Cyanopyridin-4-yl})\text{methoxy}]\text{pyrimidin-2-yl}\}$ -3-methylpiperazine-1-carboxylate (39). Compound 39 was synthesized as described for 38 using (*R*)-4- $\{[(2\text{-methylpiperazin-1-yl})\text{pyrimidin-5-yloxy}]\text{methyl}\}$ nicotinonitrile and 2,2,2-trifluoroethyl phenyl carbonate as starting materials in 39% yield: ^1H NMR (400 MHz, DMSO) δ 8.99 (s, 1H), 8.85 (d, $J = 4.9$ Hz, 1H), 8.31 (s, 2H), 7.72 (d, $J = 4.9$ Hz, 1H), 5.31 (s, 2H), 4.85–4.60 (m, 3H), 4.40–4.27 (m, 1H), 4.03–3.91 (m, 1H), 3.89–3.77 (m, 1H), 3.33–3.03 (m, 3H), 1.10 (d, $J = 6.5$ Hz, 3H); HRMS (ESI) calcd for $\text{C}_{19}\text{H}_{20}\text{O}_3\text{N}_6\text{F}_3$ ($M + \text{H}$) $^+$ 437.1543, found 437.1542.

2,2-Difluoroethyl (3*R*)-4- $\{5-[(3\text{-Cyanopyridin-4-yl})\text{methoxy}]\text{pyrimidin-2-yl}\}$ -3-methylpiperazine-1-carboxylate (40). Compound 40 was synthesized as described for 38 using (*R*)-4- $\{[(2\text{-methylpiperazin-1-yl})\text{pyrimidin-5-yloxy}]\text{methyl}\}$ nicotinonitrile and 2,2-difluoroethyl phenyl carbonate as starting materials in 10% yield: ^1H NMR (400 MHz, CDCl_3) δ 8.91 (s, 1H), 8.85 (d, $J = 5.2$ Hz, 1H), 8.18 (s, 2H), 7.71–7.61 (m, 1H), 5.97 (t, $J = 55.4$ Hz, 1H), 5.21 (s, 2H), 4.90–4.78 (m, 1H), 4.48–4.23 (m, 3H), 4.23–3.86 (m, 2H), 3.20 (td, $J = 13.1$, 3.5 Hz, 2H), 3.13–2.95 (m, 1H), 1.17 (d, $J = 6.6$ Hz, 3H); LRMS (ES^+) m/z ($M + \text{H}$) $^+$ 419.

4- $\{[(2\text{-}[(2*R*)-4-(5\text{-fluoropyrimidin-2-yl})\text{-2-methylpiperazin-1-yl}]\text{pyrimidin-5-yl}]\text{oxy}]\text{methyl}\}$ pyridine-3-carbonitrile (41). To a stirred solution of (*R*)-4- $\{[(2\text{-methylpiperazin-1-yl})\text{pyrimidin-5-yloxy}]\text{methyl}\}$ nicotinonitrile dihydrochloride (1.31 g, 3.42 mmol) and 2-chloro-5-fluoropyrimidine (0.498 g, 3.76 mmol) in acetonitrile (54 mL) in a microwave vial was added *N,N*-diisopropylethylamine (1.905 mL, 10.94 mmol). The stirred mixture was heated at 150 °C for 3 h and cooled to ambient temperature, and the reaction was diluted with EtOAc (300 mL), washed with water (150 mL) and then brine (100 mL), and evaporated in vacuo to a residue which was chromatographed on silica with 0–70% EtOAc in isohexane as the eluant to give a solid which was triturated with CH_2Cl_2 /ether to give 4- $\{[(2\text{-}[(2*R*)-4-(5\text{-fluoropyrimidin-2-yl})\text{-2-methylpiperazin-1-yl}]\text{pyrimidin-5-yl}]\text{oxy}]\text{methyl}\}$ pyridine-3-carbonitrile (400 mg, 29%): mp 140–141 °C; ^1H NMR (400 MHz, DMSO) δ 1.05 (d, $J = 6.6$ Hz, 3H), 3.04 (td, $J = 12.0$, 3.7 Hz, 1H), 3.27–3.14 (m, 2H), 4.35 (dt, $J = 13.2$, 3.1 Hz, 1H), 4.55–4.40 (m, 2H), 4.79 (ddd, $J = 6.5$, 3.9, 2.4 Hz, 1H), 5.34 (s, 2H), 7.74 (dd, $J = 5.1$, 0.6 Hz, 1H), 8.34 (s, 2H), 8.45 (d, $J = 0.8$ Hz, 2H), 8.87 (d, $J = 5.1$ Hz, 1H), 9.05 (d, $J = 0.6$ Hz, 1H); HRMS (ESI) calcd for $\text{C}_{20}\text{H}_{20}\text{ON}_8\text{F}$ ($M + \text{H}$) $^+$ 407.1739, found 407.1737.

4- $\{[(2\text{-}[(2*R*)-2\text{-Methyl-4- $\{5-(1\text{-methylethyl})\text{-1,2,4-oxadiazol-3-yl}\}$ piperazin-1-yl]pyrimidin-5-yl]oxy]methyl}\}$ pyridine-3-carbonitrile (42). (*R*)-3- $\{4-(5-[(3\text{-Bromopyridin-4-yl})\text{methoxy}]\text{pyrimidin-2-yl})\}$ -3-methylpiperazin-1-yl-5-isopropyl-1,2,4-oxadiazole (1.09 g, 2.30 mmol), zinc cyanide (0.270 g, 2.30 mmol), tris(dibenzylideneacetone)dipalladium(0) (7.80 mg, 8.52 μmol), and

xantphos (0.106 g, 0.18 mmol) were placed in a dry flask and stirred under a stream of nitrogen. After 20 min degassed DMF (1 mL) was added and the resultant black mixture degassed by vacuum/nitrogen six times. The reaction was heated to 130 °C for 165 min in an oil bath, cooled to room temperature, then diluted with CH₂Cl₂ (100 mL), and washed with 2 M K₂CO₃(aq) (50 mL). The organic layer was dried over MgSO₄, filtered, and evaporated to afford crude product as a brown oil which solidified on standing. The crude product was purified by flash silica chromatography, elution gradient 0–100% EtOAc in isohexane. Pure fractions were evaporated to dryness to afford 4-[[2-((2R)-2-methyl-4-[5-(1-methylethyl)-1,2,4-oxadiazol-3-yl]piperazin-1-yl)pyrimidin-5-yl]oxy]methyl]pyridine-3-carbonitrile (925 mg, 88%) as a very pale yellow solid: mp 117–118 °C; [α]_D¹⁸ –67.6; ¹H NMR (400 MHz, CDCl₃) δ 8.91 (s, 1H), 8.85 (d, *J* = 5.2 Hz, 1H), 8.20 (s, 2H), 7.66 (dd, *J* = 5.2, 0.6 Hz, 1H), 5.22 (s, 2H), 4.96–4.86 (m, 1H), 4.47 (ddd, *J* = 13.4, 3.3, 2.2 Hz, 1H), 4.01 (ddt, *J* = 12.4, 3.5, 1.8 Hz, 1H), 3.85 (dt, *J* = 12.6, 1.7 Hz, 1H), 3.31 (ddd, *J* = 13.4, 12.3, 3.7 Hz, 1H), 3.22 (dd, *J* = 12.7, 4.0 Hz, 1H), 3.14–2.99 (m, 2H), 1.36 (d, *J* = 7.0 Hz, 6H), 1.25 (d, *J* = 6.7 Hz, 3H); ¹³C NMR (101 MHz, CDCl₃) 183.0, 170.8, 158.0, 153.4, 153.0, 148.9, 146.6, 144.7, 121.8, 114.8, 108.1, 68.8, 50.3, 46.6, 45.9, 38.2, 27.7, 20.1 (2C), 14.3; IR (Nujol) ν_{\max} 2234, 1586, 1548, 1461, 1376, 1287, 1269, 1223, 1176, 1036, 927, 834 cm⁻¹; HRMS (ESI) calcd for C₂₁H₂₅O₂N₈ (M + H)⁺ 421.2095, found 421.2092.

4-[[2-((2R)-4-(5-Cyclopropyl-1,2,4-oxadiazol-3-yl)-2-methylpiperazin-1-yl)pyrimidin-5-yl]oxy]methyl]pyridine-3-carbonitrile (43). Compound 43 was synthesized as described for 42 using (R)-3-(4-(5-((3-bromopyridin-4-yl)methoxy)pyrimidin-2-yl)-3-methylpiperazin-1-yl)-5-cyclopropyl-1,2,4-oxadiazole as the starting material in 54% yield: mp 132–133 °C; ¹H NMR (400 MHz, DMSO) δ 9.11 (s, 1H), 8.94 (d, *J* = 5.1 Hz, 1H), 8.40 (s, 2H), 7.81 (d, *J* = 5.1 Hz, 1H), 5.40 (s, 2H), 4.98–4.74 (m, 1H), 4.52–4.34 (m, 1H), 3.88 (d, *J* = 12.5 Hz, 1H), 3.75 (d, *J* = 12.7 Hz, 1H), 3.30–3.11 (m, 2H), 3.00 (td, *J* = 12.3, 3.7 Hz, 1H), 2.29–2.14 (m, 1H), 1.23 (dt, *J* = 7.9, 3.3 Hz, 2H), 1.17 (d, *J* = 6.6 Hz, 3H), 1.13–1.07 (m, 2H).

4-[[2-((2R)-2-Methyl-4-(5-Methyl-1,2,4-oxadiazol-3-yl)piperazin-1-yl)pyrimidin-5-yl]oxy]methyl]pyridine-3-carbonitrile (44). Compound 44 was synthesized as described for 42 using (R)-3-(4-(5-((3-bromopyridin-4-yl)methoxy)pyrimidin-2-yl)-3-methylpiperazin-1-yl)-5-methyl-1,2,4-oxadiazole as the starting material in 32% yield: mp 109–110 °C; ¹H NMR (400 MHz, DMSO, 100 °C) δ 8.99 (s, 1H), 8.86 (d, *J* = 5.1 Hz, 1H), 8.31 (s, 2H), 7.72 (d, *J* = 5.1 Hz, 1H), 5.31 (s, 2H), 4.91–4.76 (m, 1H), 4.39 (dt, *J* = 13.5, 3.0 Hz, 1H), 3.85 (dd, *J* = 12.5, 1.6 Hz, 1H), 3.73 (dt, *J* = 12.8, 1.8 Hz, 1H), 3.34–3.14 (m, 2H), 3.08–2.97 (m, 1H), 2.44 (s, 3H), 1.16 (d, *J* = 6.6 Hz, 3H); HRMS (ESI) calcd for C₁₉H₂₁O₂N₈ (M + H)⁺ 393.1782, found 393.1780.

4-[[2-((2R)-2-Methyl-4-[5-(trifluoromethyl)-1,2,4-oxadiazol-3-yl]piperazin-1-yl)pyrimidin-5-yl]oxy]methyl]pyridine-3-carbonitrile (45). Cesium carbonate (5.49 g, 16.86 mmol) was added to 4-(chloromethyl)nicotinonitrile (2.14 g, 14.05 mmol) and (R)-2-(2-methyl-4-(5-(trifluoromethyl)-1,2,4-oxadiazol-3-yl)piperazin-1-yl)pyrimidin-5-ol (4.64 g, 14.05 mmol) in DMF (60 mL). The resulting mixture was stirred at 20 °C for 70 h. The reaction mixture was quenched with water (15 mL) and extracted with EtOAc (2 × 20 mL), and the organic layer was dried over MgSO₄, filtered, and evaporated to afford a beige solid that was purified by flash silica chromatography, elution gradient 10–30% EtOAc in CH₂Cl₂. The oil was triturated with isohexane/Et₂O to give a solid which was collected by filtration and dried under vacuum to give 4-[[2-((2R)-2-methyl-4-[5-(trifluoromethyl)-1,2,4-oxadiazol-3-yl]piperazin-1-yl)pyrimidin-5-yl]oxy]methyl]pyridine-3-carbonitrile (3.43 g, 55%) as a white solid: mp 83–84 °C; [α]_D¹⁸ –46.8; ¹H NMR (400 MHz, CDCl₃) δ 8.91 (s, 1H), 8.85 (d, *J* = 5.2 Hz, 1H), 8.20 (s, 2H), 7.66 (dd, *J* = 5.1, 0.7 Hz, 1H), 5.22 (s, 2H), 5.02–4.91 (m, 1H), 4.52 (ddd, *J* = 13.4, 3.2, 2.3 Hz, 1H), 4.10–3.98 (m, 1H), 3.88 (dt, *J* = 12.8, 1.7 Hz, 1H), 3.39–3.26 (m, 2H), 3.15 (td, *J* = 12.3, 3.7 Hz, 1H), 1.25 (d, *J* = 6.7 Hz, 3H); ¹³C NMR (101 MHz, CDCl₃) δ 170.4, 164.5 (q, *J* = 43.8 Hz), 157.8, 153.4, 152.9, 148.8, 146.5 (2C), 144.8, 121.8, 115.4 (q, *J* = 274.8 Hz), 114.7, 108.1, 68.8, 50.2, 46.5, 45.7, 37.8, 14.2; IR (Nujol) ν_{\max} 2234,

1615, 1583, 1274, 1163, 1088, 1061, 1035, 991, 909, 837, 791 cm⁻¹; HRMS (ESI) calcd for C₁₉H₁₈O₂N₈F₃(M + H)⁺ 447.1499, found 447.1497.

4-[[2-((2R)-4-[5-(Difluoromethyl)-1,2,4-oxadiazol-3-yl]-2-methylpiperazin-1-yl)pyrimidin-5-yl]oxy]methyl]pyridine-3-carbonitrile (46). Compound 46 was synthesized as described for 45 using (R)-2-(4-(5-(difluoromethyl)-1,2,4-oxadiazol-3-yl)-2-methylpiperazin-1-yl)pyrimidin-5-ol as the starting material in 34% yield: mp 126–127 °C; [α]_D¹⁸ –60.9; ¹H NMR (400 MHz, CDCl₃) δ 8.91 (s, 1H), 8.85 (d, *J* = 5.2 Hz, 1H), 8.20 (s, 2H), 7.66 (dd, *J* = 5.2, 0.8 Hz, 1H), 6.65 (t, *J* = 52.4 Hz, 1H), 5.22 (s, 2H), 4.87–4.85 (m, 1H), 4.56–4.47 (m, 1H), 4.07–3.98 (m, 1H), 3.88 (dt, *J* = 12.8, 1.7 Hz, 1H), 3.38–3.28 (m, 2H), 3.13 (td, *J* = 12.3, 3.7 Hz, 1H), 1.25 (d, *J* = 6.7 Hz, 3H); ¹³C NMR (101 MHz, CDCl₃) δ = 170.6, 167.4 (t, *J* = 29.5 Hz), 157.9, 153.5, 153.0, 148.8, 146.5 (2C), 144.8, 121.8, 114.8, 108.1, 105.6 (t, *J* = 244.4 Hz), 68.8, 50.3, 46.6, 45.8, 37.9, 14.3; IR (Nujol) ν_{\max} 2231, 1609, 1583, 1289, 1270, 1228, 1179, 1115, 1081, 1063, 1041, 910, 833, 822 cm⁻¹; HRMS (ESI) calcd for C₁₉H₁₈O₂N₈F₂ (M + H)⁺ 429.1594, found 429.1590.

4-[[2-((2R)-2-Methyl-4-[3-(1-methylethyl)-1,2,4-oxadiazol-5-yl]piperazin-1-yl)pyrimidin-5-yl]oxy]methyl]pyridine-3-carbonitrile (47). Compound 47 was synthesized as described for 45 using (R)-2-(4-(3-isopropyl-1,2,4-oxadiazol-5-yl)-2-methylpiperazin-1-yl)pyrimidin-5-ol as the starting material in 68% yield: mp 115–116 °C; [α]_D¹⁸ –79.2; ¹H NMR (400 MHz, CDCl₃) δ 8.91 (s, 1H), 8.85 (d, *J* = 5.2 Hz, 1H), 8.20 (s, 2H), 7.68–7.63 (m, 1H), 5.22 (s, 2H), 4.99–4.89 (m, 1H), 4.56–4.44 (m, 1H), 4.20–4.08 (m, 1H), 3.96 (dd, *J* = 14.7, 1.6 Hz, 1H), 3.41 (dd, *J* = 13.0, 4.0 Hz, 1H), 3.35–3.20 (m, 2H), 2.91 (hept, *J* = 7.0 Hz, 1H), 1.30 (d, *J* = 7.0 Hz, 6H), 1.23 (d, *J* = 6.7 Hz, 3H); ¹³C NMR (101 MHz, CDCl₃) δ 175.8, 171.4, 157.7, 153.4, 152.9, 148.7, 146.5, 144.9, 121.8, 114.7, 108.1, 68.7, 50.1, 46.5, 45.7, 37.9, 27.0, 20.4 (2C), 14.1; IR (Nujol) ν_{\max} 2230, 1621, 1592, 1552, 1460, 1408, 1347, 1281, 1265, 1222, 1180, 1034, 1017, 839 cm⁻¹; HRMS (ESI) calcd for C₂₁H₂₅O₂N₈ (M + H)⁺ 421.2095, found 421.2091.

4-[[2-((2R)-4-(3-Cyclopropyl-1,2,4-oxadiazol-5-yl)-2-methylpiperazin-1-yl)pyrimidin-5-yl]oxy]methyl]pyridine-3-carbonitrile (48). Compound 48 was synthesized as described for 45 using (R)-2-(2-methyl-4-(3-(cyclopropyl)-1,2,4-oxadiazol-5-yl)piperazin-1-yl)pyrimidin-5-ol as the starting material in 48% yield: ¹H NMR (400 MHz, CDCl₃) δ 8.91 (s, 1H), 8.85 (d, *J* = 5.2 Hz, 1H), 8.19 (s, 2H), 7.71–7.61 (m, 1H), 5.22 (s, 2H), 4.93 (ddt, *J* = 6.4, 4.1, 2.4 Hz, 1H), 4.58–4.43 (m, 1H), 4.16–4.02 (m, 1H), 3.92 (dt, *J* = 13.0, 1.7 Hz, 1H), 3.38 (dd, *J* = 13.0, 4.0 Hz, 1H), 3.35–3.14 (m, 2H), 1.88 (tt, *J* = 8.0, 5.4 Hz, 1H), 1.21 (d, *J* = 6.7 Hz, 3H), 1.01–0.91 (m, 4H); HRMS (ESI) calcd for C₂₁H₂₃O₂N₈ (M + H)⁺ 419.1938, found 419.1935.

4-[[2-((2R)-2-Methyl-4-[3-(trifluoromethyl)-1,2,4-oxadiazol-5-yl]piperazin-1-yl)pyrimidin-5-yl]oxy]methyl]pyridine-3-carbonitrile (49). Compound 49 was synthesized as described for 45 using (R)-2-(2-methyl-4-(3-(trifluoromethyl)-1,2,4-oxadiazol-5-yl)piperazin-1-yl)pyrimidin-5-ol as the starting material in 30% yield: mp 150–151 °C; ¹H NMR (400 MHz, CDCl₃) δ 8.92 (s, 1H), 8.86 (d, *J* = 5.2 Hz, 1H), 8.22 (s, 2H), 7.66 (d, *J* = 5.1 Hz, 1H), 5.23 (s, 2H), 5.07–4.96 (m, 1H), 4.65–4.51 (m, 1H), 4.26–4.12 (m, 1H), 4.01 (d, *J* = 13.1 Hz, 1H), 3.51 (dd, *J* = 13.1, 4.0 Hz, 1H), 3.41–3.25 (m, 2H), 1.24 (d, *J* = 6.8 Hz, 3H); ¹³C NMR (101 MHz, CDCl₃) 172.3, 161.9 (q, *J* = 39.0 Hz), 157.5, 153.4, 153.0, 148.6, 146.4, 145.1, 121.8, 118.1 (q, *J* = 272.1 Hz), 114.7, 108.1, 68.7, 50.3, 46.3, 45.9, 37.7, 14.0; IR (Nujol) ν_{\max} 2227, 1648, 1590, 1546, 1465, 1401, 1345, 1293, 1234, 1155, 1089, 1058, 908, 837 cm⁻¹; HRMS (ESI) calcd for C₁₉H₁₈O₂N₈F₃(M + H)⁺ 447.1499, found 447.1499.

■ ASSOCIATED CONTENT

Supporting Information

Experimental details for the syntheses of the intermediates, crystallographic information, biological protocols, and procedures for the determination of physicochemical properties. This material is available free of charge via the Internet at <http://pubs.acs.org>.

AUTHOR INFORMATION

Corresponding Author

*Phone: +44 (0)1625 232567. Fax: +44 (0)1625 516667. E-mail: jamie.scott@astrazeneca.com.

Notes

The authors declare no competing financial interest.

ACKNOWLEDGMENTS

Wendy Snelson, Helen Pointon, and Ruth Poultney are thanked for their synthetic contribution. Members of the AstraZeneca Animal Science & Welfare group are thanked both for their work on breeding the mice and for their technical support in running the experiments. Johnathan Bright is thanked for statistical analysis of the cAMP assay. Michael Waring is thanked for providing helpful comments on the manuscript, and the reviewers are thanked for constructive comments on agonist pharmacology.

ABBREVIATIONS USED

GPR119, G protein coupled receptor 119; WT, wild type; KO, knockout; OEA, oleoylethanolamide; OLDA, N-oleoyldopamine; GLP-1, glucagon-like peptide-1; PPB, plasma protein binding; LLE, ligand-lipophilicity efficiency; SAR, structure-activity relationship; hERG, human ether-a-go-go-related gene; OGTT, oral glucose tolerance test; DPP-IV, dipeptidyl peptidase-4

REFERENCES

- (1) Fredriksson, R.; Höglund, P. J.; Gloriam, D. E. I.; Lagerström, M. C.; Schiöth, H. B. Seven evolutionarily conserved human rhodopsin G protein-coupled receptors lacking close relatives. *FEBS Lett.* **2003**, *554*, 381–388.
- (2) Overton, H. A.; Babbs, A. J.; Doel, S. M.; Fyfe, M. C. T.; Gardner, L. S.; Griffin, G.; Jackson, H. C.; Procter, M. J.; Rasamison, C. M.; Tang-Christensen, M.; Widdowson, P. S.; Williams, G. M.; Reynet, C. Deorphanization of a G protein-coupled receptor for oleoylethanolamide and its use in the discovery of small-molecule hypophagic agents. *Cell Metab.* **2006**, *3*, 167–175.
- (3) Chu, Z.; Carroll, C.; Chen, R.; Alfonso, J.; Gutierrez, V.; He, H.; Lucman, A.; Xing, C.; Sebring, K.; Zhou, J.; Wagner, B.; Unett, D.; Jones, R. M.; Behan, D. P.; Leonard, J. N-Oleoylethanolamine enhances glucose homeostasis through the activation of GPR119. *Mol. Endocrinol.* **2010**, *24*, 161–170.
- (4) Chu, Z.; Carroll, C.; Alfonso, J.; Gutierrez, V.; He, H.; Lucman, A.; Pedraza, M.; Mondala, H.; Gao, H.; Bagnol, D.; Chen, R.; Jones, R. M.; Behan, D. P.; Leonard, J. A role for intestinal endocrine cell-expressed g protein-coupled receptor 119 in glycemic control by enhancing glucagon-like peptide-1 and glucose-dependent insulinotropic peptide release. *Endocrinology* **2008**, *149*, 2038–2047.
- (5) Chu, Z.; Jones, R. M.; He, H.; Carroll, C.; Gutierrez, V.; Lucman, A.; Moloney, M.; Gao, H.; Mondala, H.; Bagnol, D.; Unett, D.; Liang, Y.; Demarest, K.; Semple, G.; Behan, D. P.; Leonard, J. A role for β -cell-expressed G protein-coupled receptor 119 in glycemic control by enhancing glucose-dependent insulin release. *Endocrinology* **2007**, *148*, 2601–2609.
- (6) (a) Fyfe, M. C. T.; McCormack, J. G.; Overton, H. A.; Procter, M. J.; Reynet, C. GPR119 agonists as potential new oral agents for the treatment of type 2 diabetes and obesity. *Expert Opin. Drug Discovery* **2008**, *3*, 403–413. (b) Shah, U. GPR119 agonists: A promising new approach for the treatment of type 2 diabetes and related metabolic disorders. *Curr. Opin. Drug Discovery Dev.* **2009**, *12*, 519–532.
- (7) Jones, R. M.; Leonard, J. N. The emergence of GPR119 agonists as anti-diabetic agents. In *Annual Reports in Medicinal Chemistry*; Macor, J. E., Ed.; Academic Press: San Diego, CA, 2009; Vol. 44, Chapter 7, pp 149–170.
- (8) Semple, G.; Fioravanti, B.; Pereira, G.; Calderon, I.; Uy, J.; Choi, K.; Xiong, Y.; Ren, A.; Morgan, M.; Dave, V.; Thomsen, W.; Unett, D. J.; Xing, C.; Bossie, S.; Carroll, C.; Chu, Z.; Grottick, A. J.; Hauser, E. K.; Leonard, J.; Jones, R. M. Discovery of the first potent and orally efficacious agonist of the orphan G-protein coupled receptor 119. *J. Med. Chem.* **2008**, *51*, 5172–5175.
- (9) Semple, G.; Ren, A.; Fioravanti, B.; Pereira, G.; Calderon, I.; Choi, K.; Xiong, Y.; Shin, Y.; Gharbaoui, T.; Sage, C. R.; Morgan, M.; Xing, C.; Chu, Z.; Leonard, J. N.; Grottick, A. J.; Al-Shamma, H.; Liang, Y.; Demarest, K. T.; Jones, R. M. Discovery of fused bicyclic agonists of the orphan G-protein coupled receptor GPR119 with in vivo activity in rodent models of glucose control. *Bioorg. Med. Chem. Lett.* **2011**, *21*, 3134–3141. (b) Semple, G.; Lehmann, J.; Wong, A.; Ren, A.; Bruce, M.; Shin, Y.; Sage, C. R.; Morgan, M.; Chen, W.; Sebring, K.; Chu, Z.; Leonard, J. N.; Al-Shamma, H.; Grottick, A. J.; Du, F.; Liang, Y.; Demarest, K.; Jones, R. M. Discovery of a second generation agonist of the orphan G-protein coupled receptor GPR119 with an improved profile. *Bioorg. Med. Chem. Lett.* **2012**, *22*, 1750–1755.
- (10) Wu, Y.; Kuntz, J. D.; Carpenter, A. J.; Fang, J.; Sauls, H. R.; Gomez, D. J.; Ammal, C.; Xu, Y.; Hart, S.; Tadepalli, S. 2,5-Disubstituted pyridines as potent GPR119 agonists. *Bioorg. Med. Chem. Lett.* **2010**, *20*, 2577–2581.
- (11) (a) McClure, K. F.; Darout, E.; Guimarães, C. R. W.; DeNinno, M. P.; Mascitti, V.; Munchhof, M. J.; Robinson, R. P.; Kohrt, J.; Harris, A. R.; Moore, D. E.; Li, B.; Samp, L.; Lefker, B. A.; Futatsugi, K.; Kung, D.; Bonin, P. D.; Cornelius, P.; Wang, R.; Salter, E.; Hornby, S.; Kalgutkar, A. S.; Chen, Y. Activation of the G-protein-coupled receptor 119: A conformation-based hypothesis for understanding agonist response. *J. Med. Chem.* **2011**, *54*, 1948–1952. (b) Mascitti, V.; Stevens, B. D.; Choi, C.; McClure, K. F.; Guimarães, C. R. W.; Farley, K. A.; Munchhof, M. J.; Robinson, R. P.; Futatsugi, K.; Lavergne, S. Y.; Lefker, B. A.; Cornelius, P.; Bonin, P. D.; Kalgutkar, A. S.; Sharma, R.; Chen, Y. Design and evaluation of a 2-(2,3,6-trifluorophenyl)-acetamide derivative as an agonist of the GPR119 receptor. *Bioorg. Med. Chem. Lett.* **2011**, *21*, 1306–1309. (c) Kalgutkar, A. S.; Mascitti, V.; Sharma, R.; Walker, G. W.; Ryder, T.; McDonald, T. S.; Chen, Y.; Preville, C.; Basak, A.; McClure, K. F.; Kohrt, J. T.; Robinson, R. P.; Munchhof, M. J.; Cornelius, P. Intrinsic electrophilicity of a 4-substituted-5-cyano-6-(2-methylpyridin-3-yloxy)pyrimidine derivative: structural characterization of glutathione conjugates in vitro. *Chem. Res. Toxicol.* **2011**, *24*, 269–278. (d) Sharma, R.; Eng, H.; Walker, G. S.; Barreiro, G.; Stepan, A. F.; McClure, K. F.; Wolford, A.; Bonin, P. D.; Cornelius, P.; Kalgutkar, A. S. Oxidative metabolism of a quinoxaline derivative by xanthine oxidase in rodent plasma. *Chem. Res. Toxicol.* **2011**, *24*, 2207–2216.
- (12) (a) Xia, Y.; Chackalamannil, S.; Greenlee, W. J.; Jayne, C.; Neustadt, B.; Stamford, A.; Vaccaro, H.; Xu, X.; Baker, H.; O'Neill, K.; Woods, M.; Hawes, B.; Kowalski, T. Discovery of a nortropanol derivative as a potent and orally active GPR119 agonist for type 2 diabetes. *Bioorg. Med. Chem. Lett.* **2011**, *21*, 3290–3296. (b) Szweczyk, J. W.; Acton, J.; Adams, A. D.; Chicchi, G.; Freeman, S.; Howard, A. D.; Huang, Y.; Li, C.; Meinke, P. T.; Mosely, R.; Murphy, E.; Samuel, R.; Santini, C.; Yang, M.; Zhang, Y.; Zhao, K.; Wood, H. B. Design of potent and selective GPR119 agonists for type II diabetes. *Bioorg. Med. Chem. Lett.* **2011**, *21*, 2665–2669.
- (13) (a) Yoshida, S.; Ohishi, T.; Matsui, T.; Tanaka, H.; Oshima, H.; Yonetoku, Y.; Shibasaki, M. The role of small molecule GPR119 agonist, AS1535907, in glucose-stimulated insulin secretion and pancreatic β -cell function. *Diabetes, Obes. Metab.* **2011**, *13*, 34–41. (b) Yoshida, S.; Ohishi, T.; Matsui, T.; Tanaka, H.; Oshima, H.; Yonetoku, Y.; Shibasaki, M. Novel GPR119 agonist AS1535907 contributes to first-phase insulin secretion in rat perfused pancreas and diabetic db/db mice. *Biochem. Biophys. Res. Commun.* **2010**, *402*, 280–285. (c) Yoshida, S.; Tanaka, H.; Oshima, H.; Yamazaki, T.; Yonetoku, Y.; Ohishi, T.; Matsui, T.; Shibasaki, M. AS1907417, a novel GPR119 agonist, as an insulinotropic and β -cell preservative agent for the treatment of type 2 diabetes. *Biochem. Biophys. Res. Commun.* **2010**, *400*, 745–751. (d) Yoshida, S.; Ohishi, T.; Matsui, T.; Shibasaki, M.

Identification of a novel GPR119 agonist, AS1269574, with in vitro and in vivo glucose-stimulated insulin secretion. *Biochem. Biophys. Res. Commun.* **2010**, *400*, 437–441. (e) Negoro, K.; Yonetoku, Y.; Maruyama, T.; Yoshida, S.; Takeuchi, M.; Ohta, M. Synthesis and structure–activity relationship of 4-amino-2-phenylpyrimidine derivatives as a series of novel GPR119 agonists. *Bioorg. Med. Chem.* **2012**, *20*, 2369–2375.

(14) (a) Shah, U.; Kowalski, T. J. GPR119 agonists for the potential treatment of type 2 diabetes and related metabolic disorders. In *Vitamins & Hormones*; Litwack, G., Ed.; Academic Press: San Diego, CA, 2010; Vol. 84, pp 415–448. (b) Jones, R. M.; Leonard, J. N.; Buzard, D. J.; Lehmann, J. GPR119 agonists for the treatment of type 2 diabetes. *Expert Opin. Ther. Pat.* **2009**, *19*, 1339–1359.

(15) Zhu, X.; Huang, D.; Lan, X.; Tang, C.; Zhu, Y.; Han, J.; Huang, W.; Qian, H. The first pharmacophore model for potent G protein-coupled receptor 119 agonist. *Eur. J. Med. Chem.* **2011**, *46*, 2901–2907.

(16) (a) Mcwherter, C. A.; Martin, R. L.; Karpf, D. B.; Roberts, B. K.; Lorenz, D. A.; Ketner, R. J. Compositions of 5-ethyl-2-{4-[4-(4-tetrazol-1-yl-phenoxy)methyl]thiazol-2-yl]-piperidin-1-yl}pyrimidine. WO2011163090. (b) Nunez, D. Treatment of blood lipid abnormalities and other associated conditions using 5-[[1-[3-(1-methylethyl)-1,2,4-oxadiazol-5-yl]-4-piperidinyl]methyl]oxy]-2-[4-(methylsulfonyl)phenyl]pyridine. WO2011150067.

(17) (a) Katz, L. B.; Gambale, J. J.; Rothenberg, P. L.; Vanapalli, S. R.; Vaccaro, N.; Xi, L.; Polidori, D. C.; Vets, E.; Sarich, T. C.; Stein, P. P. Pharmacokinetics, pharmacodynamics, safety, and tolerability of JNJ-38431055, a novel GPR119 receptor agonist and potential antidiabetes agent, in healthy male subjects. *Clin. Pharmacol. Ther.* **2011**, *90*, 685–692. (b) Katz, L. B.; Gambale, J. J.; Rothenberg, P. L.; Vanapalli, S. R.; Vaccaro, N.; Xi, L.; Sarich, T. C.; Stein, P. P. Effects of JNJ-38431055, a novel GPR119 receptor agonist, in randomized, double-blind, placebo-controlled studies in subjects with type 2 diabetes. *Diabetes, Obes. Metab.* **2012**, article in press, <http://onlinelibrary.wiley.com/doi/10.1111/j.1463-1326.2012.01587.x/abstract>.

(18) Brocklehurst, K. J.; Broo, A.; Butlin, R. J.; Brown, H. S.; Clarke, D. S.; Davidsson, Ö.; Goldberg, K.; Groombridge, S. D.; Kelly, E. E.; Leach, A.; McKerrecher, D.; O'Donnell, C.; Poucher, S.; Schofield, P.; Scott, J. S.; Teague, J.; Westgate, L.; Wood, M. J. M. Discovery, optimization and in vivo evaluation of novel GPR119 agonists. *Bioorg. Med. Chem. Lett.* **2011**, *21*, 7310–7316.

(19) GPR119 agonists were tested on HEK293S cells overexpressing human GPR119. Changes in cAMP concentrations were assessed using the cAMP dynamic 2 HTRF kit (Cisbio). Cells were diluted in assay buffer (20 mM HEPES, pH 7.4, Hank's balanced salt solution, 0.01% BSA, 1 mM IBMX) and used at 2×10^3 cells/well in 384-well plates. Cells were incubated with compound for 45 min before addition of HTRF lysis and detection reagents according to the manufacturer's protocol. Fluorescence readings were captured using an Envision plate reader and cAMP concentrations calculated using a standard curve. Typical standard deviations in log EC₅₀ when a compound is repeated are 0.20 and 0.27 for the human and mouse assays, respectively. This translates to 95% of EC₅₀ values within 2.5-fold (human) and 3.5-fold (mouse) of a compound's "true" EC₅₀. The intrinsic activity was expressed as the percent effect compared to that of the control, 50 μ M oleylethanolamide, defined as 100% as per the following reference: Ariens, E. J. Affinity and intrinsic activity in the theory of competitive inhibition. I. Problems and theory. *Arch. Int. Pharmacodyn. Ther.* **1954**, *99*, 32–49.

(20) log D_{7,4} plasma–protein binding, and solubility measurements were made as described in the following reference: Buttar, D.; Colclough, N.; Gerhardt, S.; MacFaul, P. A.; Phillips, S. D.; Plowright, A.; Whittamore, P.; Tam, K.; Maskos, K.; Steinbacher, S.; Steuber, H. A. Combined spectroscopic and crystallographic approach to probing drug–human serum albumin interactions. *Bioorg. Med. Chem.* **2010**, *18*, 7486–7496.

(21) Waring, M. J. Lipophilicity in drug discovery. *Expert Opin. Drug Discovery* **2010**, *5*, 235–248.

(22) Jain, N.; Yalkowsky, S. H. Estimation of the aqueous solubility I: Application to organic nonelectrolytes. *J. Pharm. Sci.* **2001**, *90*, 234–252.

(23) Other examples of improving solubility through disruption of crystal packing include the following: (a) Wenglowksy, S.; Moreno, D.; Rudolph, J.; Ran, Y.; Ahrendt, K. A.; Arrigo, A.; Colson, B.; Gloor, S. L.; Hastings, G. Pyrazolopyridine inhibitors of B-Raf^{V600E}. Part 3: An increase in aqueous solubility via the disruption of crystal packing. *Bioorg. Med. Chem. Lett.* **2012**, *22*, 912–915. (b) Ishikawa, M.; Hashimoto, Y. Improvement in aqueous solubility in small molecule drug discovery programs by disruption of molecular planarity and symmetry. *J. Med. Chem.* **2011**, *54*, 1539–1554. (c) Lanier, M. C.; Moorjani, M.; Luo, Z.; Chen, Y.; Lin, E.; Tellew, J. E.; Zhang, X.; Williams, J. P.; Gross, R. S.; Lechner, S. M.; Markison, S.; Joswig, T.; Kargo, W.; Piercey, J.; Santos, M.; Malany, S.; Zhao, M.; Petroski, R.; Crespo, M. I.; Díaz, J. -L.; Saunders, J.; Wen, J.; O'Brien, Z.; Jalali, K.; Madan, A.; Slee, D. H. N-[6-Amino-2-(heteroaryl)pyrimidin-4-yl]-acetamides as A2A receptor antagonists with improved drug like properties and in vivo efficacy. *J. Med. Chem.* **2009**, *52*, 709–717. (d) Fujita, Y.; Yonehara, M.; Tetsushashi, M.; Noguchi-Yachide, T.; Hashimoto, Y.; Ishikawa, M. β -Naphthoflavone analogs as potent and soluble aryl hydrocarbon receptor agonists: Improvement of solubility by disruption of molecular planarity. *Bioorg. Med. Chem.* **2010**, *18*, 1194–1203.

(24) Our survey found 58 relevant structures that were available at that time. These were classified as being involved in interactions such as the head-to-head interaction that links the blue molecule in Figure 1c with the molecule immediately to the right and ladder-type interactions if they resembled those linking the blue molecule to the molecule above and to the right. Some were involved in both kinds of interactions in a fashion similar to that of molecule 2. It was found that of the 57 structures that we could classify (one structure, RAHYOP, involved a more complex array of interactions and was not included in this analysis) 10 (18%) were involved in head-to-head interactions, 10 (18%) were involved in ladder interactions, and 13 (23%) featured both types of interaction. The remaining 24 structures (42%) did not feature any of these interactions involving the sulfone.

(25) Urgaonkar, S.; Verkade, J. Palladium/proazaphosphatranecatalyzed amination of aryl halides possessing a phenol, alcohol, acetanilide, amide or an enolizable ketone functional group: Efficacy of lithium bis(trimethylsilyl)amide as the base. *Adv. Synth. Catal.* **2004**, *346*, 611–616.

(26) Leeson, P. D.; Springthorpe, B. The influence of drug-like concepts on decision-making in medicinal chemistry. *Nat. Rev. Drug Discovery* **2007**, *6*, 881–890.

(27) The use of LLE in an agonist program has the potential to be misleading if not considered in conjunction with intrinsic activities to account for the magnitude of the agonist response and pharmacology (e.g., partial vs full agonists). We did however find the concept of LLE useful in terms of keeping lipophilicity at the forefront of our thinking when optimizing potency. For a recent example of LLE being used without an inhibitor/antagonist context see: Waring, M. J.; Johnstone, C.; McKerrecher, D.; Pike, K. G.; Robb, G. Matrix-based multi-parameter optimization of glucokinase activators: The discovery of AZD1092. *Med. Chem. Commun.* **2011**, *2*, 775–779.

(28) The reduction in lipophilicity observed when replacing a N with a CH may seem counterintuitive, but in this case it may be explained on the basis of electronic interactions and proximity corrections that need to be taken into account when the piperazine N is located in the 2-position of the pyrimidine, which renders the piperazine more lipophilic than would be expected from fragment values alone. For further discussion see: (a) Leo, A. The octanol-water partition coefficient of aromatic solutes: The effect of electronic interactions, alkyl chains, hydrogen bonds, and ortho-substitution. *J. Chem. Soc., Perkin Trans. 2* **1983**, 825–838. (b) Lewis, S. J.; Mirrlees, M. S.; Taylor, P. J. Rationalisations among heterocyclic partition coefficients part 2: The azines. *Quant. Struct.-Activ. Relat.* **1983**, *2*, 100–111. (c) Mannhold, R.; Rekker, R. The hydrophobic fragmental constant approach for calculating log P in octanol/water and aliphatic

hydrocarbon/water systems. *Perspect. Drug Discovery Des.* **2000**, *18*, 1–18.

(29) This is expected for groups adjacent to a nitrogen which is attached to an electron-withdrawing exocyclic substituent. For this kind of nitrogen, the exocyclic bond has partial double bond character, and $A_{1,3}$ strain about this partial double bond makes the equatorial position the most sterically crowded. This is reinforced by the fact that the nitrogen three bonds away from the methyl substituent does not have an axial group and so does not contribute to transannular steric crowding.

(30) Meanwell, N. A. Synopsis of some recent tactical application of bioisosteres in drug design. *J. Med. Chem.* **2011**, *54*, 2529–2591.

(31) Ertan, A.; Goldberg, K.; Groombridge, S.; Hudson, J.; Leach, A. G.; Pickup, A.; Poultney, R.; Scott, J. S.; Svensson, P. H.; Sweeney, J.; MacFaul, P. A. Oxadiazole isomers: All bioisosteres are not created equal. *Med. Chem. Commun.* **2012**, *3*, 600–604.

(32) hERG measurements were made as described in the following reference: Bridgland-Taylor, M. H.; Hargreaves, A. C.; Easter, A.; Orme, A.; Henthorn, D. C.; Ding, M.; Davis, A. M.; Small, B. G.; Heapy, C. G.; Abi-Gerges, N.; Persson, F.; Jacobson, I.; Sullivan, M.; Albertson, N.; Hammond, T. G.; Sullivan, E.; Valentin, J. -P.; Pollard, C. E. Optimisation and validation of a medium-throughput electrophysiology-based hERG assay using IonWorks HT. *J. Pharmacol. Toxicol. Methods* **2006**, *54*, 189–199.

(33) All in vivo studies were randomized, blocked across test days when a study had to be run over 2 d, and designed to have 80% power to detect effects of the desired size. A positive control was used to monitor the reproducibility of the models. GLP-1 data were log transformed. ANOVA with contrasts was used where appropriate to compare groups of interest. ANCOVA with contrasts was used where necessary to adjust for the covariate baseline levels (for glucose) or day effects when a study was split over 2 d. Where LS means are shown, this indicates that ANCOVA has been used. Significance is denoted as follows: *, $p < 0.05$; **, $p < 0.01$; ***, $p < 0.001$.

(34) Deacon, C. F. Dipeptidyl peptidase-4 inhibitors in the treatment of type 2 diabetes: A comparative review. *Diabetes, Obes. Metab.* **2011**, *13*, 7–18.